



# Geology and fluid inclusion geochemistry of the Zijinshan high-sulfidation epithermal Cu-Au deposit, Fujian Province, SE China: Implication for deep exploration targeting



Jun Zhong<sup>a,b</sup>, Yan-Jing Chen<sup>b,\*</sup>, Jing Chen<sup>b,c</sup>, Jin-Ping Qi<sup>d</sup>, Mao-Chang Dai<sup>d</sup>

<sup>a</sup> Beijing Research Institute of Uranium Geology, Beijing 100029, China

<sup>b</sup> Key Laboratory of Orogen and Crust Evolution, Peking University, Beijing 100871, China

<sup>c</sup> Centre of Excellence in Ore Deposits, University of Tasmania, Hobart, Tasmania 7001, Australia

<sup>d</sup> Zijin Mining Group Co. Ltd, Shanghang 364200, Fujian, China

## ARTICLE INFO

### Keywords:

Fluid inclusion

Vapor CO<sub>2</sub>-rich magmatic fluids

Epithermal-porphyry mineralization system

Zijinshan high-sulfidation epithermal Cu-Au deposit

Mineral exploration

## ABSTRACT

The giant Zijinshan Cu-Au deposit in the Zijinshan orefield, Fujian Province, southeastern China, is the first high-sulfidation epithermal deposit identified in mainland China. The Cu and Au orebodies occur as veins and pods in the NW-trending faults and breccias zones. Intensive and pervasive alteration is characterized by downward and outward zoning from intensively leached silicic alteration (or vuggy quartz, Q), through alunite-quartz-pyrite alteration (advanced argillic alteration, Q-Alu) and the quartz-alunite alteration overprinting the sericite alteration (Q-Alu-Di-Srt), to sericite (or phyllic) alteration zone. Gold mineralization mainly occurs in the silicic alteration zone, while the copper mineralization is confined in the alunite-quartz alteration zone. On the basis of detailed petrographic study, an early porphyry type mineralization stage, characterized by chalcopyrite-bornite-molybdenite-pyrite-sericite assemblage is recognized at Zijinshan, which is subsequently and strongly overprinted by the sulfate alteration and high-sulfidation Cu-Au mineralization stages. A supergene stage is also identified at shallow depth of the deposit, with gold largely enriched but copper commonly leached. The ore-forming fluids related to the early sericite alteration and possibly porphyry type mineralization are high-temperature, high-salinity magmatic water, characterized by the presence of the halite-bearing inclusions. The CO<sub>2</sub>-H<sub>2</sub>O (C-type) inclusions are mostly vapor-rich and abundantly identified in the samples with advanced argillic alteration (alunite alteration). They are regarded to be the buoyant vapor phase by fluid boiling of a single-phase, low- to moderate-salinity magmatic fluid at depth, where a separated saline phase and related porphyry mineralization might be expected. A group of secondary inclusions coexisting with enargite grains are recognized in the samples with alunite alteration and suggested to be trapped from the ore-forming fluids of the Cu-Au mineralization stage. The total homogenization temperatures and salinities of the secondary inclusions are below 300 °C (peaking at 260–280 °C) and under 10 wt% NaCl eqv., respectively. Intensive fluid boiling is the major mechanism for the formation of the giant high-sulfidation Cu (covellite-, digenite-dominated) orebodies in the Zijinshan deposit. It is a deep-seated high-sulfidation epithermal deposit according to the estimated depth of 1.4–2.1 km from the C-type inclusions in quartz grains from the alunite alteration zone. By fluid inclusion mapping of a nearly NW-trending cross section profile, the isotherms are extrapolated using the average total homogenization temperatures and the possible heat source is suggested. It is indicated that the heat source and possible concealed porphyry mineralization nearly coeval to the high-sulfidation Cu-Au mineralization at Zijinshan might be located at the southeastern Zijinshan deposit or the northern area between the Zijinshan and Wuziqilong deposits, where deep drilling is encouraged.

## 1. Introduction

Epithermal deposits are important sources of copper, gold, silver, lead and zinc, which can be further classified into the high-sulfidation

(HS) and low-sulfidation (LS) subtypes in terms of the diagnostic gangue mineral assemblages, sulfide assemblages and contents (Simmons et al., 2005; Hedenquist et al., 2000; Hedenquist, 1987; Heald et al., 1987; Pirajno, 2009; Chen et al., 2012). South China is an

\* Corresponding author at: Department of Geology, Peking University, Beijing 100871, China.  
E-mail address: [yjchen@pku.edu.cn](mailto:yjchen@pku.edu.cn) (Y.-J. Chen).

important epithermal metallogenic province and hosts at least 43 epithermal deposits, of which the Zijinshan Cu-Au deposit in Fujian Province is the first and only typical HS deposit (Zhong et al., 2017a). Since its discovery in 1980s, > 300 t gold (at 0.53 g/t) and 2.32 Mt copper (at 0.36%) have been identified in the Zijinshan Cu-Au deposit (Zhang, 2013), making it the first discovered as well as the largest epithermal gold-copper deposit in mainland China. Former publications about the Zijinshan deposit focus on ore geology (Chen, 1999; Zhang et al., 1992; So et al., 1998), mineralogy (Qiu et al., 2010; Wang and Jue, 2013; Liu et al., 2011, 2016), fluid geochemistry (Zhang et al., 1992; So et al., 1998) and geochronology (Zhang et al., 1992; Chen, 1996; Zhou and Chen, 1996) of the samples collected from shallow parts of the deposit. Recent drilling by the Zijin Mining Group revealed covellite- and digenite-dominated mineralization at depth of  $-400$  m above sea level (asl), indicating its vertical Au-Cu mineralization extended  $> 1500$  m (from  $\sim 1100$  m to  $-400$  m asl). The mineralogy of both the ore (Cu-sulfides) and gangue minerals (e.g., alunite) at depth had been studied (Qiu et al., 2010; Wang and Jue, 2013; Liu et al., 2011, 2016), yet the ore-forming fluid geochemical features have not been detailedly investigated and the genesis of the thick orebodies remains unclear. Moreover, concealed porphyry mineralization at depth in Zijinshan has been suggested by many researchers (Qiu et al., 2010; Zhang, 2013; Liu et al., 2016) by the comparison with other porphyry-epithermal mineralization systems (e.g., Sillitoe, 2010; Hedenquist and Lowenstern, 1994; Heinrich, 2005), but the exact possible target locations of the porphyry mineralization have not been predicted yet.

In this contribution, we present the systematic fluid inclusion results, especially for those samples collected from the deep part (below  $+520$  m or  $+330$  m asl) of the Zijinshan deposit, and further discuss the hydrothermal fluid evolution and ore mineral precipitation processes. By vertical fluid inclusion mapping, we have determined the possible heat source of the ore-forming fluids, and predicted the possible location of the concealed porphyry deposit at depth.

## 2. Regional geology

The Zijinshan orefield, the most well-developed porphyry-epithermal mineralization system in China (Zhong et al., 2017c), includes at least the Luoboling porphyry Cu-Mo deposit (Zhong et al., 2011, 2014, 2017a), the Yueyang LS Ag-Cu-Pb-Zn polymetallic deposit (Zhang et al., 2003a; Zhong et al., 2017b), the Wuziqilong Cu deposit (Chen et al., 2011), the Longjiangting Cu deposit (Chen et al., 2015; Chen, 2013), and several other occurrences (Zhang et al., 2003b). The orefield is located to the northeast of the NW-trending Shanghang-Yunxiao deep fault in southwestern Fujian Province (Fig. 1; Zhong et al., 2014, 2017b, 2017c). The major lithostratigraphic units herein include the metamorphic rocks of the Neoproterozoic Louziba Group, the Late Paleozoic clastic sediments, the Early Cretaceous volcanic assemblages and the Quaternary alluvial sediments. The oldest Louziba Group is composed of low-grade metamorphic shallow-marine sediments, including two-mica schist, muscovite schist, phyllite, metasiltstone and metasandstone. The Late Paleozoic rocks are divided into the Late Devonian Tianwadong and Taozikeng Formations and Early Carboniferous Lindi Formation. These formations comprise coastal to shallow marine facies siltstone, sandstone and conglomerate, and are locally intercalated with marl and felsic tuff. The Early Cretaceous Shimaoshan Group, unconformably overlying the above-mentioned rocks, includes dacite, rhyolite, ignimbrite and tuff, with minor conglomerate intercalations (Zhong et al., 2011, 2014).

The pre-Mesozoic rocks were folded into a NE-trending anticline which was intruded by Yanshanian granitoids along the axis (Fig. 1). The Yanshanian granitoids contain the Middle-Late Jurassic and Early Cretaceous granitic intrusions, including: (1) Middle Jurassic Zijinshan granite batholiths with SHRIMP U-Pb zircon age of  $168 \pm 4$  Ma (Zhao et al., 2008) and LA-ICP-MS U-Pb zircon ages between 165 and 155 Ma (Jiang et al., 2013; Li et al., 2015); (2) Late Jurassic Caixi monzogranite

pluton yielding a SHRIMP zircon U-Pb age of  $150 \pm 3$  Ma (Zhao, 2007); (3) Early Cretaceous Sifang granodiorite pluton yielding a SHRIMP zircon U-Pb age of  $107.8 \pm 1.2$  Ma, a hornblende Ar-Ar plateau age of  $104.8 \pm 0.8$  Ma (Mao et al., 2002), and a LA-ICP-MS zircon U-Pb age of  $112 \pm 1$  Ma (Jiang et al., 2013); (4) cryptoexplosive breccia pipes and granodioritic or dacitic porphyries outcropped in the Luoboling, Zijinshan and Ermiaogou deposits, with LA-ICP-MS zircon U-Pb ages ranging from  $110 \pm 0.4$  Ma to  $103.1 \pm 1.1$  Ma (Hu et al., 2012; Jiang et al., 2013; B. Li et al., 2013; Li and Jiang, 2015); and (5) small-size granitic porphyries as exemplified by the quartz syenite porphyry in the Jintonghu deposit yielding two LA-ICP-MS zircon U-Pb ages of  $95.3 \pm 0.9$  Ma and  $96.7 \pm 0.9$  Ma (Wu et al., 2013). The Early Cretaceous porphyries and breccia pipes show a close spatial, temporal and genetic relationship with the porphyry-epithermal mineral system (So et al., 1998; Zhang et al., 2001; Zhong et al., 2014, 2017a, 2017c). Previous researches suggest that the mineralization is mainly controlled by the NW faults, while the NE-trending faults controlled the emplacement of the intrusions in the Zijinshan Orefield (e.g., Zhang et al., 1992; So et al., 1998).

## 3. Deposit geology

The Zijinshan Cu-Au deposit is located at the center of the Zijinshan orefield (Fig. 1). The Middle Jurassic Zijinshan granitic complex is the oldest lithologic unit in the mining area (Fig. 2), and mainly includes the Jingmei coarse-grained cataclastic granite, the Wulongzi medium- to fine-grained biotite granite and the Jinlongqiao fine-grained muscovite granite. The medium- to fine-grained biotite granite is most widespread in the Zijinshan deposit and is the major host rock for the Cu-Au orebodies. The Middle Jurassic Zijinshan granitic rocks show geochemical characteristics of the S-type granite and are regarded to be derived from partial melting of the Mesoproterozoic basement rocks, yielding LA-ICP-MS U-Pb zircon ages from 165 to 155 Ma (Jiang et al., 2013; Li et al., 2015). An Early Cretaceous volcanic dome complex was recognized in the ore district, consisting of the central pipelike dacitic porphyry and surrounding cryptoexplosive breccias, tuff and lava (Fig. 2). Besides the breccia pipe surrounding the dacitic porphyry, a series of NW-trending breccia veins also occurred to the northwest of the volcanic dome (Fig. 2), and were favorable for Cu-Au mineralization. Jiang et al. (2017) recently reported a Re-Os isochron age of  $103 \pm 4$  Ma for seven pyrite samples, which is nearly coeval to the Cu-related alunite  $^{40}\text{Ar}-^{39}\text{Ar}$  age ( $\sim 103$  Ma, our unpublished data in Zhong et al., 2017a). These isotopic ages are slightly later than the host dacite porphyry in the Zijinshan deposit ( $105.0 \pm 0.7$  Ma and  $105.0 \pm 2.2$  Ma, Hu et al., 2012), showing intimate spatial-temporal relationship between the Cu-Au mineralization and dacite porphyry.

All the magmatic rocks in the Zijinshan Cu-Au deposit are intensively and pervasively altered, and a typical high-sulfidation alteration zonation is recognized, including the silicic alteration zone (vuggy quartz zone, Q), the quartz-alunite zone (advanced argillic zone, Q-Alu), the quartz-alunite alteration overprinting the sericite alteration zone (Q-Alu-Di-Srt), and the sericite alteration zone (Phy). The Q zone occurs in the middle and shallower part (mostly above  $+650$  m asl) of the ore district, which gives way downward and outward through the Q-Alu zone and the Q-Alu-Di-Srt zone, to the Phy zone (Fig. 2). The Q zone is characterized by the vuggy quartz ores (Fig. 3a, b, c) formed by acid leaching and later supergene oxidation, with diagnostic mineral assemblage of fine-grained quartz ( $> 90\%$  in volume), limonite, goethite, jarosite, and dickite (or kaolinite). Economic gold orebodies are confined in the Q zone, consisting of native gold, minor pyrite and minor secondary covellite, malachite. The Q-Alu zone is spatially associated with the Cu mineralization in the Zijinshan deposit and mainly contains hypogene platy alunite, quartz, pyrite, dickite, and minor sericite (Fig. 4c, f). The dickite contents increases downward and a narrow dickite alteration zone is suggested by Zhang et al. (1992) and So et al. (1998). The major ore minerals in the Q-Alu zone include

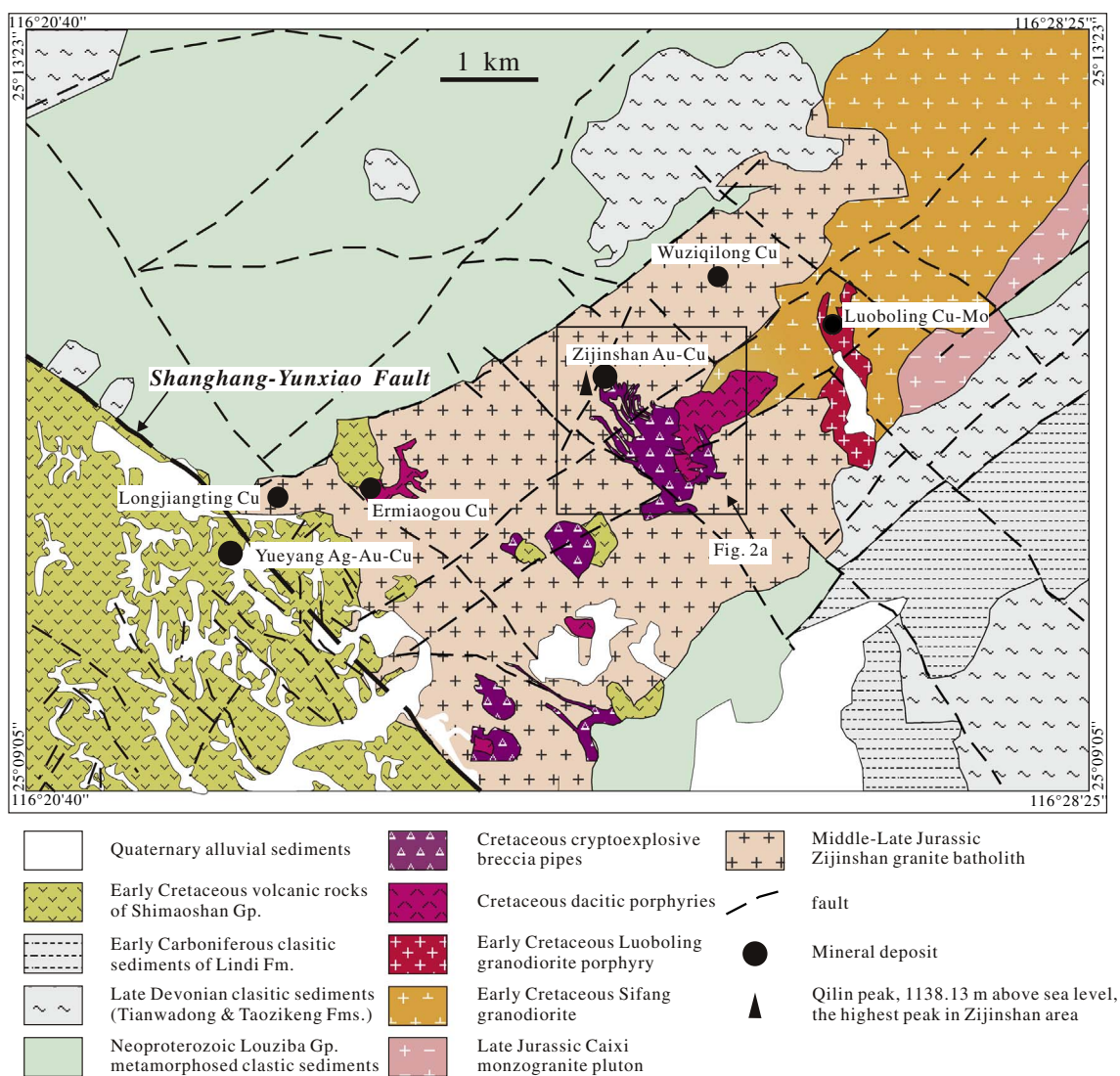


Fig. 1. Geological map of the Zijinshan Orefield. (Modified after Zhong et al. (2014).)

covellite, digenite, enargite, minor chalcopyrite, bornite (Fig. 5b–h, j–k) and a variety kinds of tin-sulfide (Fig. 5g; Liu et al., 2016). The Phy alteration zone is mainly composed of quartz, sericite, pyrite (Fig. 4b), while the Q-Alu-Di-Srt zone contains quartz, alunite, dickite, sericite (Fig. 4d, e). Minor covellite and digenite are identified in both the Phy and Q-Alu-Di-Srt alteration zones. By detailed field investigation, drill core logging and petrographic observations, it is suggested that the sericite alteration is the earliest and overprinted by alunite alteration and dickite alteration (Fig. 4d, e).

Both the Cu and Au mineralization in the Zijinshan deposit mainly occur within the NW-trending hydrothermal breccias and veins in the northwest part of the ore district (Figs. 2, 3d, g), controlled by a series of NW-trending faults, fractures, fissures or joints. The Au ores are mainly consisted of typically vuggy quartz (Fig. 3a, b), controlled by fractures and/or hydrothermal breccias. The fragments of the breccias are mainly the silicified host granite or dacitic porphyry, while the mineralized matrix includes quartz, limonite, goethite and minor covellite (Fig. 3c). The Cu ores in the Zijinshan deposit mainly occur in veins or stockworks (Fig. 3d, f, g) and hydrothermal breccias (Fig. 3e, h). The Cu ore veins vary from several millimeters to tens of centimeters in width (Fig. 3d, f, g), and are mainly consisted of dickite, pyrite, covellite, digenite, enargite (Fig. 5c–f), crosscutting and postdating the altered host rocks with alunite + pyrite + quartz assemblages. The

fragments of the Cu-bearing breccias range from several to tens of centimeters in diameter and mainly comprises of the altered granitic rocks, while the matrix is consisted of very fine-grained dickite, alunite, quartz, pyrite and Cu-sulfides including covellite, digenite and enargite and rock flour of host rocks (Fig. 3e, h).

#### 4. Sampling and analytical methods

More than ninety samples of ores and host rocks were collected from drill core Nos. DZK801, DZK702 and DZK1202 (locations in Fig. 2) in the Zijinshan high sulfidation Cu-Au deposit, which were drilled from +520 m (DZK801, DZK1202) or +330 m (DZK702) to nearly –300 m asl. Seventy double-polished thin sections (0.03 mm thick) were made for petrologic study, using both optical and electron microprobes. Fifty double-polished thin sections (~0.3 mm thick) were made for fluid inclusion study, and eighteen of them (listed in Table 1) were chosen for microthermometric and laser Raman spectroscopic analyses.

The electron microprobe microanalyses of minerals were carried out on a JEOL JXA-8100 electron microprobe in the Key Laboratory of Orogen and Crust Evolution, Peking University. Operating conditions were 20 kV accelerating voltage, 10 nA beam current with 10 s measurement time and 1 μm spot size. Natural and synthetic minerals by

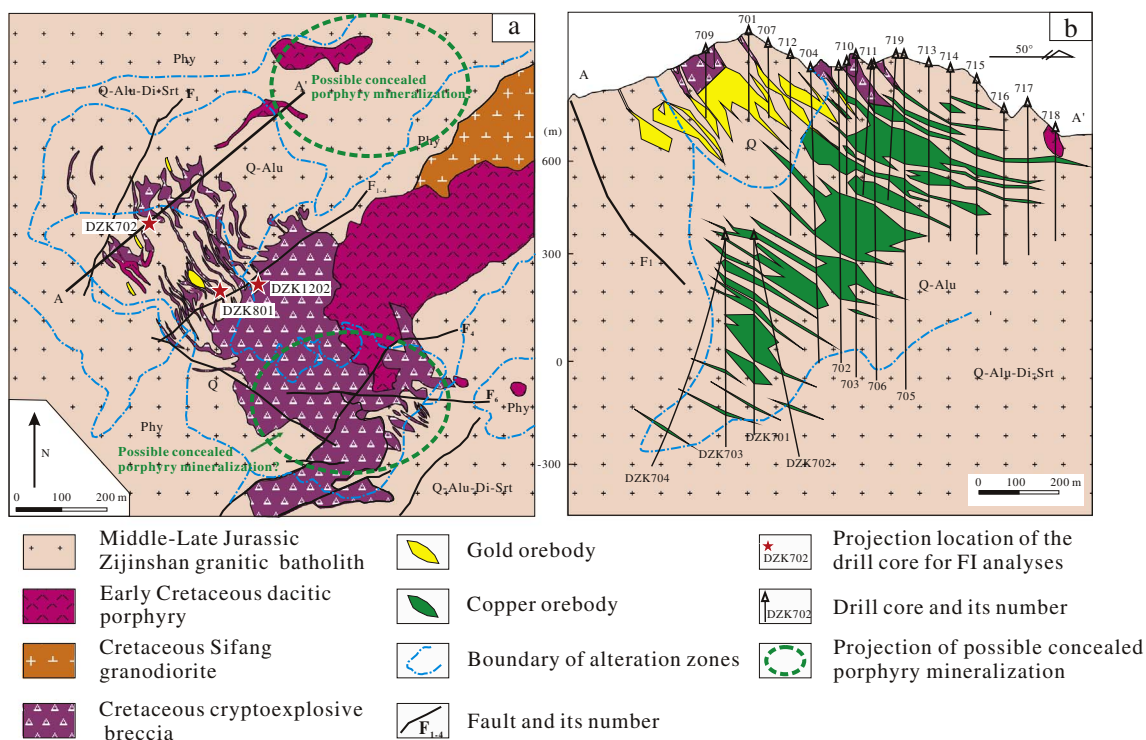


Fig. 2. Geological map of the Zijinshan Cu-Au deposit (a) and cross section profile of exploration No. 7 (b) (modified after unpublished data from Zijin Mining Group Co., Ltd., 2001). Abbreviations: Q, silicic alteration zone (vuggy quartz zone); Q-Alu, quartz-alunite zone (advanced argillic zone); Q-Alu-Di-Srt, quartz-alunite alteration overprinting the sericite alteration; Phy, sericite alteration zone (or phyllic alteration zone).

the American SPI were used as standards. The ZAF method was used for data reduction for sulfides.

Microthermometric measurements were carried out using a Linkam THMSG 600 freezing-heating stage at the Institute of Geology and Geophysics, Chinese Academy of Sciences (IGGCAS), Beijing. Temperatures were calibrated using synthetic fluid inclusions provided by FLUID INC, USA. The precisions for the measured temperatures are estimated better than  $\pm 0.5$ ,  $\pm 0.2$ , and  $\pm 2$  °C at the temperature ranges of  $-120$  to  $-70$  °C,  $-70$  to  $100$  °C, and  $100$  to  $500$  °C, respectively. During freezing/heating runs, the freezing/heating rates were constrained at  $0.5$  to  $10$  °C/min, and reduced to  $0.5$ – $1$  °C/min near phase transformation points. Salinities (reported in wt% NaCl eqv.) and densities ( $\text{g}/\text{cm}^3$ ) of the aqueous ( $\text{NaCl}-\text{H}_2\text{O}$ ) and carbonic ( $\text{CO}_2-\text{H}_2\text{O}$ ) inclusions were calculated based on final ice points (Bodnar, 1993) and the final temperatures of  $\text{CO}_2$ -clathrate (Collins, 1979) using the program Flicor (Brown, 1989).

Laser Raman spectroscopic (LRS) analyses were performed at the Key Laboratory of Orogen and Crust Evolution, Peking University, Beijing. The laser source was an argon laser with wave length of  $514.5$  nm and a source power of  $1000$  mW. Integration time was  $10$  s, with ten accumulations for each spectral line. The spectral resolution is  $\pm 2$   $\text{cm}^{-1}$  with a beam size of  $2$   $\mu\text{m}$ .

## 5. Mineral paragenesis

On the basis of ore fabrics, mineral assemblage, and crosscutting relationships, at least three mineralization stages are identified in the Zijinshan Cu-Au deposit: the porphyry, the high-sulfidation and the supergene enrichment mineralization stages, of which the high sulfidation mineralization stage can be further divided into the sulfate alteration and Cu-Au mineralization substages (Fig. 6).

The porphyry mineralization stage is characterized by the occurrence of chalcopyrite, bornite, pyrite, and rare molybdenite (Fig. 5h, i–l, Table 2), accompanied by the sericite-dominated alteration (Fig. 5l) or alunite alteration overprinting the sericite alteration (Fig. 4e) in the

same ore samples. The chalcopyrite-bornite-pyrite  $\pm$  molybdenite mineral assemblage is common all over the orefield, including the Luoboling Cu-Mo (Zhong et al., 2011, 2014, 2017c), Wuziqilong Cu (Chen et al., 2011), Longjiangting Cu-Au (Chen et al., 2015) and even the Yueyang Ag-Au-Cu (Zhong et al., 2017b) deposits. Therefore, it is indicated that the porphyry mineralization stage is resulted from a period of hydrothermal activities all over the orefield (Zhong et al., 2017b). Although the porphyry type mineral assemblages are observed in the Zijinshan deposit, they are mostly surrounded or overprinted by the later high-sulfidation mineralization and limited in scale.

The sulfate alteration substage is represented by the presence of alunite-pyrite-quartz assemblage (Figs. 4c, e, 5b), with minor pyrophyllite, diaspore, rutile (Fig. 5b), sericite and/or dickite. The silicic alteration is slightly later or nearly synchronous with the alunite alteration, predominantly consisted of fine-grained quartz and located in shallower parts (above  $+650$  m asl). The sulfate alteration substage is followed by a Cu-Au mineralization stage, consisting of native gold, covellite, digenite, enargite, anilite, gerite, djurleite and minor Sn-sulfides, sphalerite, galena (Fig. 5; Table 2). Major gangue minerals accompanying the Cu-Au ore minerals are dickite (Fig. 5d, e, f, i), quartz and minor alunite. The Cu-Au minerals are mostly in veins, stockworks, or in the matrix of the hydrothermal breccias (Fig. 3).

The Au-Cu mineralization above modern water table (above  $+650$  m asl) at Zijinshan is subsequently oxidized and leached by the circulating meteoric water. The primary Cu-minerals, including digenite, enargite and hypogene covellite are mostly leached, while the native gold (Fig. 5a) is further enriched, accompanied by limonite, goethite, jarosite, quartz and minor secondary covellite.

## 6. Fluid Inclusion study

Eighteen samples, either vein-type or disseminated ores or host rocks related to different alteration, were selected for fluid inclusion petrographic and microthermometric studies (Table 1). Abundant fluid inclusions (FIs) are identified in euhedral to subhedral quartz crystals

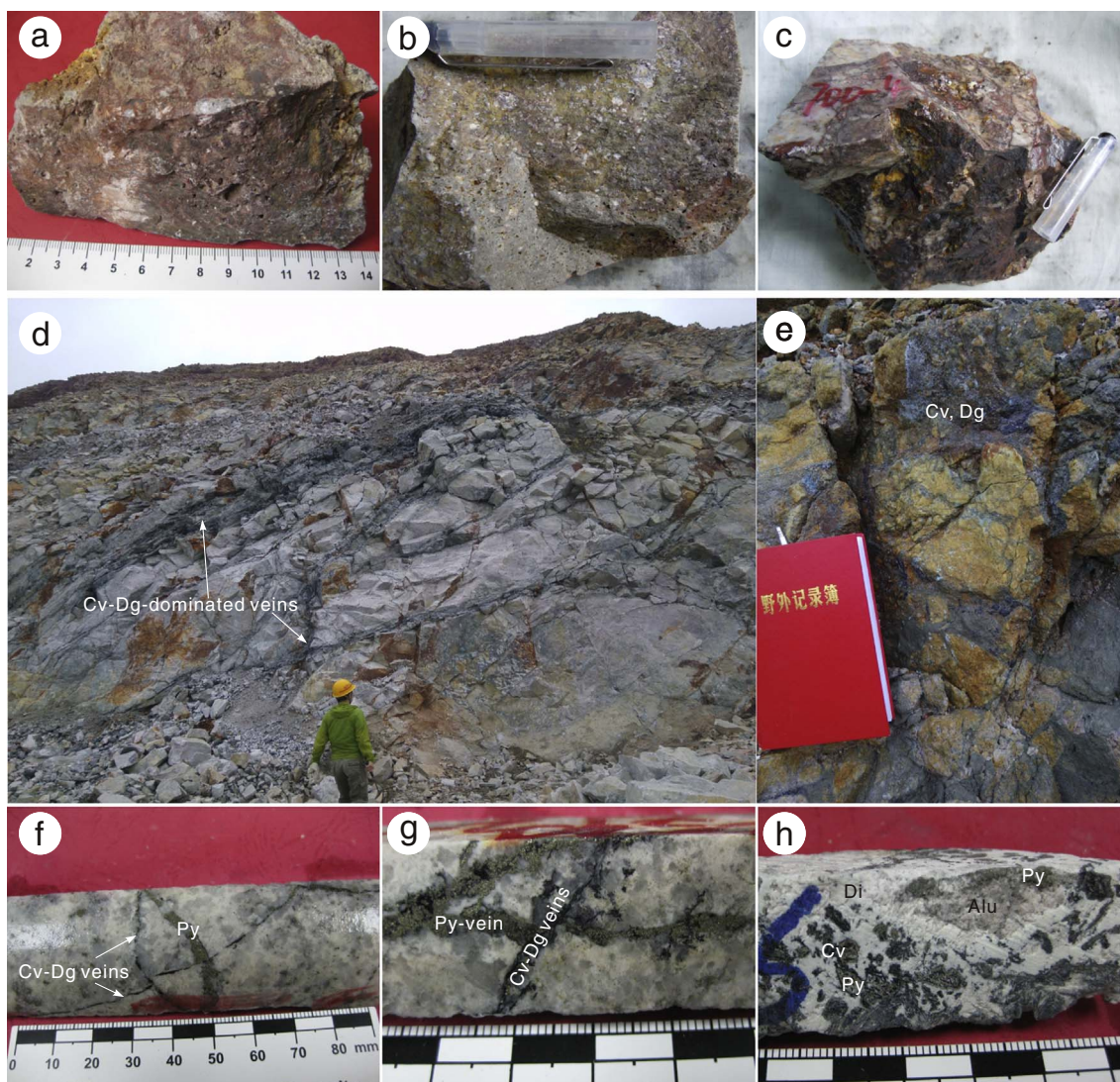


**Fig. 3.** Cu and Au ores of the Zijinshan deposit.

(a) Oxidized and leached gold ore showing vuggy quartz textures, with fine-grained quartz accounting for > 90% by volume and gold grade ~ 1–2 g/t. (b) Typical vuggy quartz ore. Coarse voids are produced by the removal of feldspar and partly filled by dickite or kaolinite. The average grade of this type ore is < 1 g/t. (c) Breccia type gold ores. The fragments are highly silicified, while the matrix is comprised of fine-grained quartz and iron oxide. (d) Cu ore veins with widths ranging from several to tens of centimeters, cutting and postdating the Zijinshan granite with advanced argillic alteration (alunite alteration). (e) Breccia type copper ores, with fragments of the altered granite and matrix of fine-grained pyrite, covellite, digenite, quartz and dickite. (f) Covellite- and digenite-bearing Cu ore stockworks cut the pyrite ± chalcopyrite veins in the alunite alteration zone. (g) Covellite-digenite ore veins cutting the pyrite veins in the alunite alteration zone. (h) Breccia type Cu ore, comprising of the granite fragment with alunite alteration and matrix composed of dickite, pyrite, covellite, digenite and minor enargite.

Abbreviations: Alu, alunite; Cv, covellite; Dg, digenite; Di, dickite; Py, pyrite.

from different alteration assemblages, i.e. the sericite-, alunite- and dickite-dominated alteration assemblages.

### 6.1. Types of fluid inclusions

On the basis of their compositions (Chen et al., 2007) and phases at room temperatures (21 °C) (Lu et al., 2004), three types of FIs were identified, namely: the aqueous (W-type), CO<sub>2</sub>-H<sub>2</sub>O (C-type) and solid-bearing type (S-type) inclusions.

The aqueous (W) type FIs are two-phase (liquid and vapor water) NaCl-H<sub>2</sub>O systems (Fig. 7a–c) and can be found in all the analyzed samples in the Zijinshan deposit. They are further divided into liquid-rich (WL) and vapor-rich (WV) subtypes according to vapor/(vapor + liquid) [V/(V + L)] ratio and homogenization mode. WL-subtype FIs, commonly with 10–45 vol% vapor phase, are common (> 70% in all the samples) in the Zijinshan deposit and all homogenized into a liquid phase. These FIs are usually round, ellipsoid, negative crystal in

shape and 5–16 μm in size (Fig. 7a–c). WV-subtype FIs are less common (usually < 30% in proportion) but observed in most samples. The WV-subtype inclusions, with V/(V + L) ratio > 60%, range from 5 to 15 μm in dimensions and are round and negative crystal in shapes (Fig. 7b), and all homogenized into vapor phase on heating run. Besides the WL- and WV-subtype FIs, pure liquid (Fig. 7c) or vapor (Fig. 7b) aqueous inclusions were also identified. The pure liquid aqueous inclusions are commonly hosted in the microfractures between quartz grains together with minor WL-subtype FIs (Fig. 7c) and regarded as secondary in origin. The pure vapor aqueous inclusions are found to be intergrown with the WV-subtype inclusions in certain quartz grains (Fig. 7b).

The carbonic (C) type FIs are two-phase (CO<sub>2</sub> + H<sub>2</sub>O) CO<sub>2</sub>-H<sub>2</sub>O system and only recognized in the alunite-dominated samples. They are ellipsoid, negative crystal or irregular in shape and 5–25 μm in size. Most (> 80%) of them have CO<sub>2</sub> phases of 60–90% in volume (Fig. 7d, e) and homogenized into vapor upon heating, while few of them with

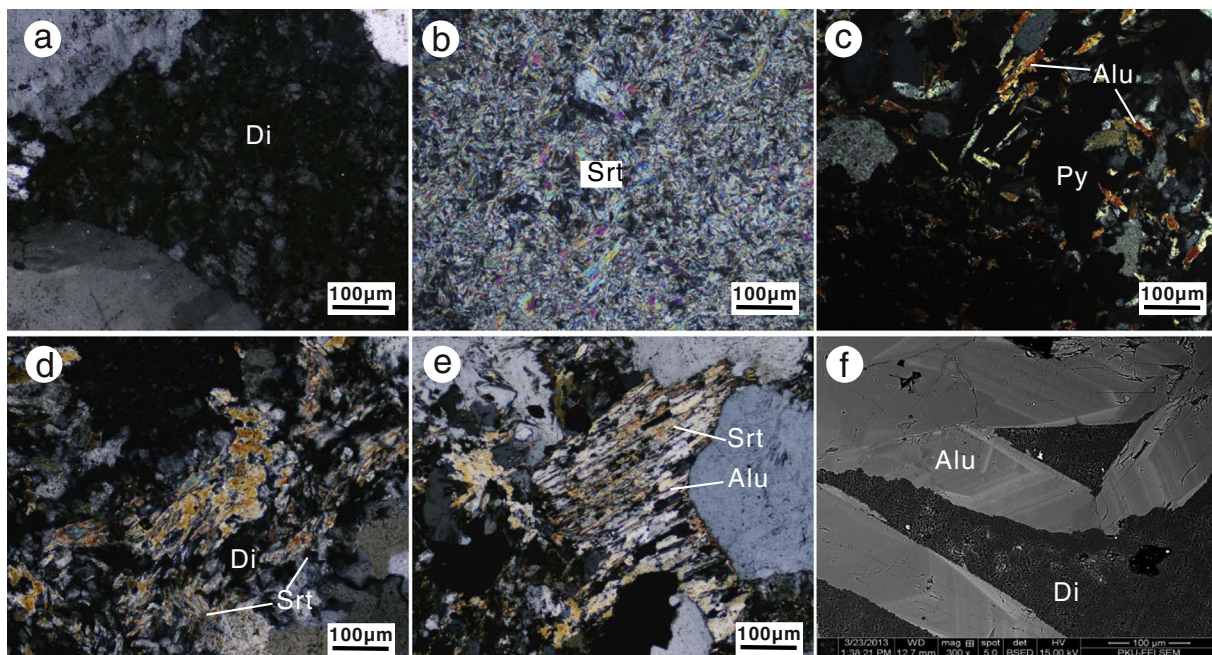


Fig. 4. Major gangue minerals in different alteration zones.

(a) Fine-grained dickite aggregates replace feldspar in host granite (crossed polars). (b) Sericite aggregates in the sericite alteration zone (crossed polars). (c) Platy alunite intergrown with pyrite in the alunite alteration zone (crossed polars). (d) Dickite replacing sericite along microfractures (crossed polars). (e) Platy alunite replacing sericite in the alunite alteration zone (crossed polars). (f) Fine-grained dickite surrounding euhedral alunite plate (backscatter electron image). Abbreviations: Alu, alunite; Di, dickite; Py, pyrite; Qtz, quartz; Srt, sericite.

CO<sub>2</sub> phases < 40% (Fig. 7f) homogenized into liquid. The “double-eyelid” texture is identified for most C-type inclusions (Fig. 7d–f). Three pure CO<sub>2</sub> inclusions (PC-type) in negative crystal shape were recognized in the Zijinshan Cu-Au deposit, ranging from 8.7, 9.7 and 10.2 µm in size, respectively. The phase boundaries of the PC-type inclusions all too vague to get systematic microthermometric results. Both the C-type and PC-type inclusions are either isolated or occur in the growth zone in quartz, implying a primary origin.

The solid-bearing (S) type FIs refer to the daughter mineral-bearing FIs, consisting of one or more daughter minerals. They are ellipsoidal or negative crystal in shape and 5–20 µm in size, which can be observed in both the alunite- and sericite-dominated alteration samples. As revealed by laser Raman spectroscopy analysis, the vapor bubbles of the S-type inclusions are either H<sub>2</sub>O or CO<sub>2</sub>. The S-type inclusions with CO<sub>2</sub> vapor phase are rare and termed as the SC-subtype. They commonly have an opaque daughter mineral (Fig. 7e) that do not disappear during heating. The S-type FIs with H<sub>2</sub>O bubble are further divided into the SH- and SM-subtypes in terms of halite presence or absence. The SH-subtype refers to the inclusions with a transparent halite (Fig. 7i), probably accompanied by other minerals including sylvite (Fig. 7g), and unidentified opaque or transparent ones (Fig. 7h). The SM-subtype inclusions, however, contain opaque and/or transparent unknown daughter mineral, but no halite daughter mineral. The SH-subtype FIs are only observed and analyzed in the sericite-dominated samples, while the SM-subtype FIs with sylvite and/or other opaque daughter minerals are recognized in both the sericite- and alunite-dominated samples. Because the opaque minerals neither disappear upon heating, nor affect the vapor and liquid phase changes in the host inclusions, the SM- and SC-subtype FIs with only an opaque daughter mineral are treated as the W- and C-type inclusions during microthermometric measurement and data processing.

## 6.2. Laser Raman spectroscopy analysis

To constrain the fluid compositions of inclusions, representative FIs were analyzed using laser Raman spectroscopy.

In the W-type FIs, the vapor and liquid phases are dominated by H<sub>2</sub>O (Fig. 8a, c, d). The liquid phase of some W-type FIs in quartz from the alunite-dominated samples contains SO<sub>4</sub><sup>2-</sup>, as indicated by the peak of 982 cm<sup>-1</sup> (Fig. 8d).

In the C-type FIs, abundant CO<sub>2</sub> is detected, supported by the diagnostic peaks of 1284 cm<sup>-1</sup> and 1388 cm<sup>-1</sup> (Fig. 8b, c). The liquid phase also contains some CO<sub>3</sub><sup>2-</sup> and H<sub>2</sub>O (Fig. 8c). Although not detected, small amounts of other gases (e.g., CH<sub>4</sub>) might be present in certain C-type FIs as supported by the maximum clathrate-melting temperatures exceeding 10 °C (Diamond, 2001).

The vapor phase of the S-type FIs is composed of H<sub>2</sub>O and CO<sub>2</sub>. The commonly observed irregular or round opaque daughter minerals are too small to be detected.

In summary, the laser Raman spectroscopy analysis indicated that the ore-forming fluids of the Zijinshan Cu-Au deposit are very complex in composition and at least contain Na<sup>+</sup>, K<sup>+</sup>, Cl<sup>-</sup>, SO<sub>4</sub><sup>2-</sup>, CO<sub>3</sub><sup>2-</sup>, CO<sub>2</sub> and H<sub>2</sub>O, etc.

## 6.3. Microthermometry

Microthermometric measurements were carried out on > 800 FIs from the sericite-dominated (porphyry mineralization-related), the alunite-dominated and dickite-dominated (associated to the high-sulfidation Cu-Au mineralization) samples. The results are summarized in Table 3 and Figs. 9, 10, and discussed as follows.

Quartz in the sericite-dominated samples contains FIs of WL-, WV-, C-, SH-, SC- and SM-subtype. The WL-subtype FIs yielded ice-melting temperatures from -13.9 to -0.2 °C, with corresponding salinities of 0.4–12.4 wt% NaCl eqv. They homogenized into liquid at temperatures of 158–446 °C, with calculated densities ranging from 0.51 to 0.92 g/cm<sup>3</sup>. The WV-subtype FIs are ellipsoidal and irregular in shape and iced at temperatures of -2.5 to -0.2 °C, with salinities of 0.7 to 9.9 wt% NaCl eqv. They finally homogenized into vapor at temperatures of 212 to 458 °C, with densities of 0.47 to 0.85 g/cm<sup>3</sup>. The C-type inclusions are rare in the sericite-dominated samples, with solid CO<sub>2</sub> melting, clathrate-melting and total homogenization temperatures ranging from

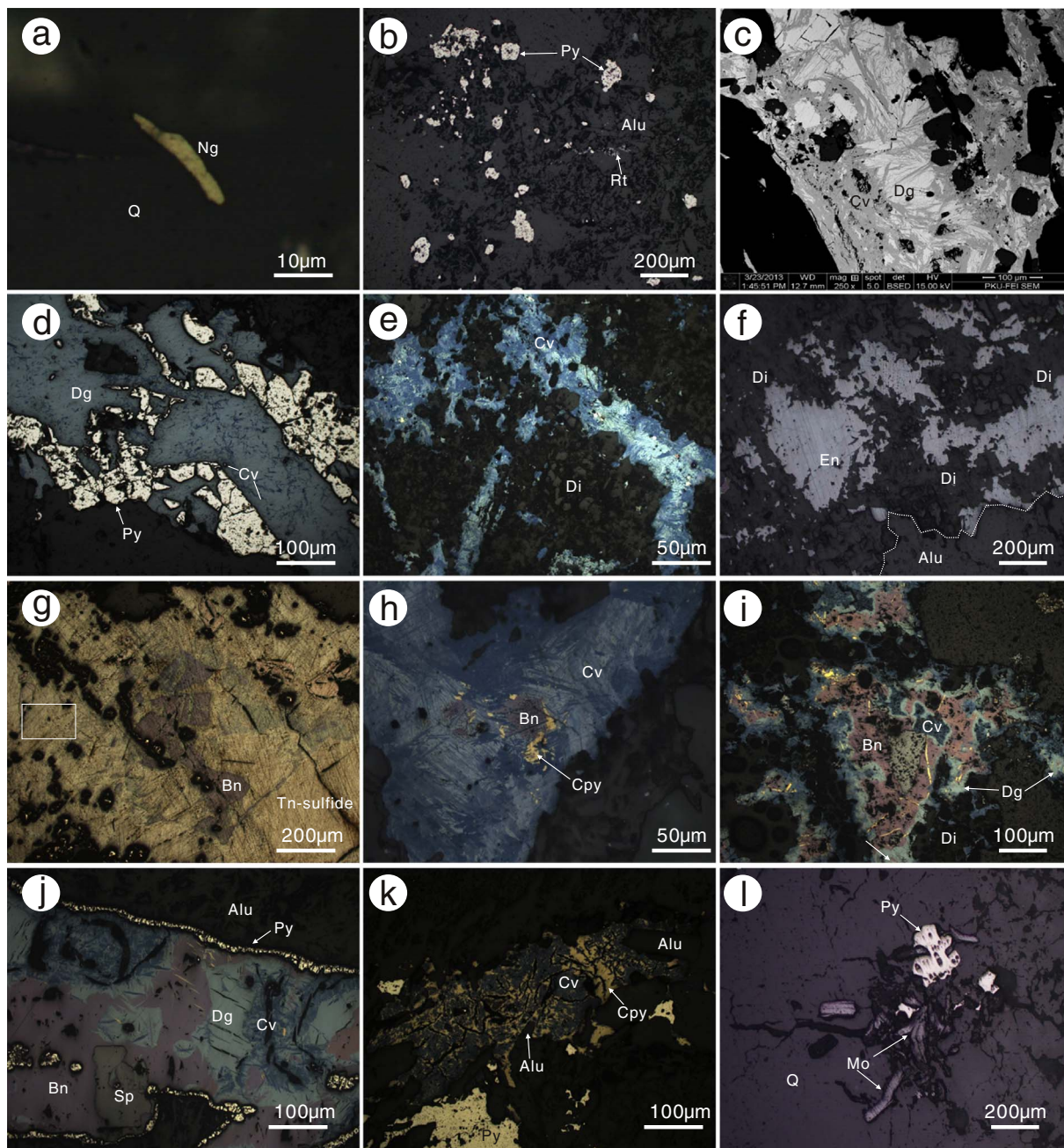


**Fig. 5.** Major ore minerals in the Zijinshan Cu-Au deposit.

(a) Native gold grain in the vuggy quartz zone. (b) Subhedral-anhedral pyrite grains intergrown with platy alunite and minor rutile residual. (c) Covellite replaces digenite in the Cu ore vein. (d) Pyrite is replaced by digenite, where fine covellite exsolution occurred. (e) Covellite intergrown with dickite in the Cu ore vein. (f) Enargite coexisting with dickite in the Cu ore vein in the alunite alteration zone, suggesting that the Cu-Au mineralization postdated the sulfate alteration. (g) Sn-sulfide replaces and surrounds bornite and fine-grained anhedral pyrite. (h) Covellite replaces and surrounds bornite and chalcopyrite, showing two-stage mineralization events. (i) Covellite and digenite replacing and surrounding bornite and exsolved chalcopyrite blade. Also shown is the sphalerite intergrown with covellite. (j) Cu-sulfides replaces pyrite in the alunite alteration zone. A pyrite boundary between Cu-sulfides and alunite plates indicates that they are formed by varied ore-forming fluids in different mineralization stages. (k) Covellite replacing chalcopyrite along intergranular microfractures. Also shown are minor alunite plates replacing chalcopyrite. (l) Molybdenite-pyrite-quartz vein develops at nearly  $-200$  m above sea level (asl) in drill core No. DZK1202.

Abbreviations: Alu, alunite; Bn, bornite; Cpy, chalcopyrite; Cv, covellite; Dg, digenite; Di, dickite; En, enargite; Mo, molybdenite; Ng, native gold; Py, pyrite; Q, quartz; Rt, rutile; Sp, sphalerite.

$-56.8$  to  $-56.6$  °C,  $5.7$ – $8.8$  °C and  $262$ – $421$  °C, corresponding to salinities and densities of  $2.4$ – $8.0$  wt% NaCl eqv. and  $0.39$ – $0.52$  g/cm<sup>3</sup>, respectively. The SH-subtype inclusions are only observed and measured in the sericite-dominated samples. Halite crystals disappeared at temperatures of  $213$  to  $393$  °C during heating, yielding salinities of  $32.5$  to  $46.7$  wt% NaCl eqv.. They all homogenized into liquid by halite dissolution with total homogenization temperatures ranging from  $213$

to  $393$  °C, and the densities ranging from  $1.07$  to  $1.13$  g/cm<sup>3</sup>. The SC-subtype FIs are all vapor-rich and homogenized into vapor at  $366$ – $388$  °C. The solid CO<sub>2</sub> melted at  $-56.8$  to  $-56.6$  °C and the clathrate-melting temperatures range from  $5.7$  to  $8.1$  °C, corresponding to salinities and densities of  $3.8$ – $8.0$  wt% NaCl eqv. and  $0.40$ – $0.44$  g/cm<sup>3</sup>. The SM-subtype FIs mostly homogenized into vapor at temperatures from  $170$  to  $389$  °C. Their ice-melting temperatures vary from

**Table 1**

Geological characteristics of selected samples from the Zijinshan Cu-Au deposit for fluid inclusion and Laser Raman spectroscopic studies.

Sample no.	Sample location (above sea level)	Dominated alteration	Mineral assemblage	Host mineral	Analyzing method
ZJ1-1	DZK801, + 506 m	Sericite	Srt, Qtz, Alu	Qtz	FI, LRS
ZJ1-5	DZK801, + 394 m	Alunite	Alu, Qtz, Srt, containing Py-Cv vein	Qtz	FI, LRS
ZJ1-11	DZK801, + 296 m	Sericite	Srt, Qtz, Alu, Di, containing Py-Cv-Dg vein	Qtz	FI, LRS
ZJ1-13	DZK801, + 184 m	Alunite	Alu-Qtz alteration halo of the Qtz-Py vein	Qtz	FI, LRS
ZJ1-20	DZK801, - 46 m	Dickite	Di, Qtz, Alu, containing Py-Dg-Cv vein	Qtz	FI, LRS
ZJ2-2	DZK1202, + 504 m	Alunite	Alu, Qtz, (disseminated) Cv, Dg	Qtz	FI, LRS
ZJ2-5	DZK1202, + 441 m	Alunite	Alu, Qtz, Di, (disseminated) Cv, Dg	Qtz	FI, LRS
ZJ2-10	DZK1202, + 366 m	Sericite	Srt, Alu, Qtz, containing Py vein	Qtz	FI
ZJ2-13	DZK1202, + 283 m	Sericite	Srt, Alu, Qtz, (disseminated) Py	Qtz	FI, LRS
ZJ2-17	DZK1202, + 155 m	Alunite	Alu, Qtz, (disseminated) Cv, Dg	Qtz	FI, LRS
ZJ2-21	DZK1202, + 65 m	Sericite	Srt, Alu, Qtz, (disseminated) Py	Qtz	FI, LRS
ZJ2-31	DZK1202, - 178 m	Sericite	Srt, Qtz, Di, Alu	Qtz	FI, LRS
ZJ2-33	DZK1202, - 253 m	Sericite	Srt, Di, Alu, Py-Qtz vein	Qtz	FI, LRS
ZJ4-7	DZK702, + 240 m	Alunite	Alu, Qtz	Qtz	FI
ZJ4-9	DZK702, + 161 m	Alunite	Alu, Qtz, Di, containing Py vein	Qtz	FI, LRS
ZJ4-10	DZK702, + 114 m	Alunite	Alu, Qtz, Di, containing Py-Cv vein	Qtz	FI
ZJ4-12	DZK702, + 26 m	Dickite	Di, Alu, Qtz, containing Py vein	Qtz	FI
ZJ4-16	DZK702, - 118 m	Sericite	Srt, Qtz, Py	Qtz	FI

Abbreviations: Alu-alunite; Cv-covellite; Di-dickite; Dg-digenite; Srt-sericite; Py-pyrite; Qtz-quartz; FI-fluid inclusion microthermometry; LRS-Laser Raman spectroscopy.

	porphyry mineralization stage	high-sulfidation epithermal mineralization stage		supergene enrichment stage
		sulfate alteration	Cu-Au mineralization	
Pyrite				
Chalcopyrite				
Bornite				
Molybdenite				
Digenite				
Covellite				
Enargite				
Sphalerite				
Galena				
Tn-sulfides				
Native gold				
Limonite				
Goethite				
Quartz				
Alunite				
Sericite				
Dickite				
Pyrophyllite				
Diaspore				
Jarosite				

**Fig. 6.** Mineral paragenesis of the Zijinshan Cu-Au deposit.

– 8.2 to – 0.1 °C, with calculated salinities of 0.2 to 11.9 wt% NaCl eqv. and densities of 0.64–0.90 g/cm<sup>3</sup>. Both the small opaque daughter minerals in the SC- and SM-subtype FIs do not disappear upon heating.

The alunite-dominated alteration samples sometimes contain Cu-sulfide ore veins and are dominated by the WL-, C-, WV-, and SM-, SC-subtype FIs. The WL-subtype FIs all homogenized into liquid at temperatures ranging from 169 to 442 °C. The ice-melting temperatures range from – 0.1 to – 10.0 °C, yielding corresponding salinities and densities of 0.2–13.9 wt% NaCl eqv. and 0.52–0.94 g/cm<sup>3</sup>, respectively. Six WV-subtype FIs all homogenized into vapor at temperatures from 280 to 382 °C, yet the ice-melting temperatures are not determined due to the vague liquid-vapor phase boundaries (Fig. 7b). The C-type and

SC-subtype FIs are abundant in the alunite alteration samples and yield solid CO<sub>2</sub> melting temperatures of – 57.7 to – 56.6 °C, below the triple-phase point of CO<sub>2</sub>, indicating the existence of minor components other than CO<sub>2</sub> dissolved in the carbonic phase (Lu et al., 2004). Their clathrate-melting temperature, calculated salinities and densities are 1.1–9.6 °C, 0.2–15.3 wt% NaCl eqv. and 0.29–1.01 g/cm<sup>3</sup>, respectively. The C-type and SC-subtype inclusions mostly homogenized into vapor, but few of them homogenized into liquid or by critical behavior at temperatures of 210–424 °C. The SM-subtype FIs all homogenized into liquid at 168–383 °C, with ice-melting temperatures, salinities and densities ranging from – 0.8 to – 9.8 °C, 1.4–13.7 wt% NaCl eqv, 0.61–0.95 g/cm<sup>3</sup>, respectively. It is worth noting that the FIs in the alunite-dominated samples are clustered in two groups in the total homogenization temperature (Th) histogram (Fig. 9), namely peaking at 320–360 °C and 240–260 °C, which is suggested to be resulted from the superposition of two-stage ore-forming fluids and will be discussed in Section 7.2.

The FIs in dickite-dominated samples are predominately the WL-subtype inclusions, with minor WV-subtype and C-type ones. The WL-subtype inclusions all homogenized into liquid at temperatures of 158–391 °C. Their ice-melting temperatures are between – 0.5 and – 5.1 °C, with salinities of 0.9–8.0 wt% NaCl eqv. and densities of 0.58–0.93 g/cm<sup>3</sup>. Only one WV-subtype inclusion yields ice-melting temperature of – 0.8 °C and total homogenization temperature of 350 °C. The C-type FIs have solid CO<sub>2</sub> melting temperatures, clathrate-melting temperatures and total homogenization temperatures of – 56.8 to – 56.6 °C, 1.5–9.9 °C and 238–334 °C, with salinities and densities of 2.6–6.6 wt% NaCl eqv. and 0.85–0.91 g/cm<sup>3</sup>, respectively. Most of the inclusions in the dickite-dominated samples homogenized below 300 °C, peaking at 260–280 °C (Fig. 9), which is consistent with the thermal stability of dickite (Hedenquist et al., 2000 and reference therein).

The microthermometric results indicated that the ore-forming fluids varied in different alteration samples (Figs. 9, 10 and Table 3). The ore-forming fluids related to the sericite alteration are of high-temperature, high-salinity, and characterized by the occurrence of the SH-subtype and minor C- and SC-subtype FIs. The ore-forming fluids resulting in the alunite alteration are featured by the presence of abundant vapor-rich C-type and SC-subtype inclusions, with total homogenization temperatures and salinities close to those of the sericite alteration. The ore-forming fluids for the dickite alteration, however, are dominated by the WL-subtype inclusions, with low temperatures and low salinities.

**Table 2**  
Electron probe microanalysis of major ore minerals in the Zijinshan deposit (wt%).

Stage	Mineral	Calculated molecular formula	Fe	As	S	Ni	Pb	Cu	Ag	Zn	Cd	Au	Sb	Total	
Porphyry mineralization stage	Pyrite	FeS <sub>2</sub>	45.59	0.04	53.98	0.02	0.13	2.81	0.08	0	0	0	0	101.65	
	Pyrite	FeS <sub>2</sub>	46.6	0	54.26	0	0.13	0.43	0	0	0	0	0	100.41	
	Pyrite	FeS <sub>2</sub>	42.39	0	54.11	0.04	0.1	0.4	0.04	0	0.06	0.25	0	100.38	
	Pyrite	FeS <sub>2</sub>	42.49	0.06	54.67	0	0.08	0.57	0.01	0	0.04	0	0.02	100.93	
	Pyrite	FeS <sub>2</sub>	46.62	0.07	52.87	0.08	0.08	0.29	0.02	0.04	0	0	0	100.07	
	Pyrite	FeS <sub>2</sub>	47.12	0	51.93	0	0.16	0.79	0.01	0	0	0	0	100	
	Chalcocopyrite	FeCuS <sub>2</sub>	29.43	0	35.59	0.03	0	32.45	0.01	0	0	0.01	0	100.52	
	Bornite	Cu <sub>5</sub> FeS <sub>4</sub>	11.13	0	25.58	0	0.04	62.38	0.02	0.03	0	0	0	99.18	
	Bornite	Cu <sub>5</sub> FeS <sub>4</sub>	11.37	0.01	25.68	0	0.01	62.51	0.09	0	0.04	0.1	0.01	99.81	
	Bornite	Cu <sub>5</sub> FeS <sub>4</sub>	11	0.03	25.63	0	0.1	65.01	0.04	0	0.01	0.04	0	101.85	
	Bornite	Cu <sub>5</sub> FeS <sub>4</sub>	11.25	0	25.35	0	0.04	64.23	0.06	0.05	0.03	0.24	0.02	100.27	
	Bornite	Cu <sub>5</sub> FeS <sub>4</sub>	11	0	25.36	0.02	0.04	64.4	0.05	0.03	0	0	0.03	99.91	
	Cu-Au mineralization stage	Digenite	Cu <sub>1.77</sub> S	2.93	0	21.6	0.03	0.13	76.61	0.27	0	0	0	0	101.58
		Digenite	Cu <sub>1.77</sub> S	2.81	0.04	21.64	0	0	72.43	0.16	0	0.01	0.13	0	101.23
		Digenite	Cu <sub>1.78</sub> S	0.27	0.06	21.84	0	0.06	77.58	0.08	0	0.02	0	0	99.9
		Digenite	Cu <sub>1.84</sub> S	0.09	0	21.25	0	0.08	78.41	0.1	0.03	0.03	0	0	99.98
Digenite		Cu <sub>1.84</sub> S	0.06	0.08	20.76	0.03	0	72.43	0.09	0.02	0	0	0.01	97.47	
Digenite		Cu <sub>1.88</sub> S	0.02	0.06	20.88	0.02	0.05	78.69	0.07	0	0	0.18	0	99.97	
Anilite		Cu <sub>1.73</sub> S	0.02	0	22.32	0.04	0.1	77.25	0.08	0	0	0	0	99.82	
Anilite		Cu <sub>1.74</sub> S	0.08	0	22.38	0	0.07	77.74	0.08	0	0.01	0	0	100.34	
Anilite		Cu <sub>1.76</sub> S	0.67	0	22.04	0.01	0.05	77.47	0	0.01	0.02	0	0.02	100.29	
Covellite		CuS	0.27	0.01	32.61	0.03	0	66.8	0.07	0.02	0	0.06	0	99.87	
Covellite		Cu <sub>1.03</sub> S	0.1	0.06	32.47	0	0.07	67.07	0.15	0	0.01	0	0	99.92	
Covellite		CuS	0	0.07	33.09	0	0	67.71	0.09	0	0	0	0	100.96	
Geerite		Cu <sub>1.58</sub> S	0.14	0.1	24.76	0.01	0.04	75.19	0.1	0.02	0.01	0.09	0	99.44	
Djurleite		Cu <sub>1.86</sub> S	0	0.01	20.93	0.03	0	77.95	0.14	0	0	0.3	0.04	99.39	
Djurleite		Cu <sub>1.96</sub> S	11.05	0	25.53	0	0.02	62.93	0.02	0	0	0.16	0	99.7	
Djurleite		Cu <sub>1.90</sub> S	47.31	0.01	52.73	0	0.14	0.12	0	0.02	0.03	0.12	0	100.48	
Enargite		Cu <sub>3</sub> AsS <sub>4</sub>	0.91	19.22	30.22	0	0.03	42.18	0.04	7.76	0.16	0	0.12	100.65	
Enargite		Cu <sub>3</sub> AsS <sub>4</sub>	0.31	19.67	32.88	0	0.07	47.53	0.05	0	0	0	0.31	100.83	
Enargite		Cu <sub>3</sub> AsS <sub>4</sub>	0.11	20.45	32.82	0.03	0.08	47.48	0.01	0.03	0.01	0	0.25	101.27	
Enargite		Cu <sub>3</sub> AsS <sub>4</sub>	0	19.81	32.35	0	0.18	47.94	0.06	0.09	0.03	0.12	0.23	100.8	
Enargite		Cu <sub>3</sub> AsS <sub>4</sub>	0.03	19.74	31.96	0.02	0.14	47.33	0.02	0.11	0	0	1.22	100.57	
Sphalerite		ZnS	0	0	32.93	0	0.05	0	0	67.14	0.48	0.2	0.01	100.81	
Sphalerite		ZnS	0	0	32.67	0	0.04	0.09	0.04	66.89	0.45	0.07	0	100.24	
Sphalerite		PbS	0.21	0	12.95	0	85.21	1.78	0.01	0	0.01	0	0	100.16	

#### 6.4. Trapping pressure and mineralization depth

According to partial and total homogenization temperatures, and the ratios of vapor CO<sub>2</sub> of the C-type FIs, the minimum trapping pressures and the isochrones of the FIs can be estimated using the Flincor program (Brown, 1989) and the formula of Bowers and Helgeson (1983) for the H<sub>2</sub>O-CO<sub>2</sub>-NaCl system. Abundant C-type FIs are recognized in the Cu-bearing ore samples with alunite alteration, which can be used for the estimation of the trapping pressures and mineralization depth. Taking the average total homogenization temperature of 320 ± 25 °C into calculation, the average trapping pressures are estimated to be 14.0–58.3 MPa (Fig. 11).

Considering the characteristics in the magmatic-epithermal environment (Fournier, 1999), i.e., pulsating hydraulic broken-and-healing caused by fluid boiling and precipitation, the fluid system can be interpreted as a state of frequent alternations between supralithostatic to lithostatic and hydrostatic pressures. Therefore, the lowest trapping pressure of FIs represents the hydrostatic system, whereas the highest trapping pressure reflects the lithostatic to supralithostatic system. Given the average density of the host granitic rocks to be 2.85 g/cm<sup>3</sup>, the corresponding depths of the alunite alteration samples range from 1.4 to 2.1 km, which were nearly identical to those of the nearby Luoboling porphyry Cu-Mo deposit (1.0–2.8 km, Zhong et al., 2014). The estimated depths of the Zijinshan deposit indicated that it is a deep-seated high-sulfidation epithermal deposit with mineralization depth exceeding the maximum depth of most other epithermal mineralization systems (< 1.5 km, Hedenquist et al., 2000; Simmons et al., 2005), even considering the estimation deviations of the pressures and depths. The great depths are favorable for the preservation of the Cu-Au orebodies and indicated that the Cu-Au mineralization at Zijinshan

might be the product of multistage mineralization events.

## 7. Discussion

### 7.1. Sources of CO<sub>2</sub> related to the alunite alteration

The carbonic inclusions (C-type and SC-subtype) are mostly common in the alunite-dominated samples. They are mostly vapor CO<sub>2</sub>-rich that can be formed by (1) interaction between the acidic ore-forming fluids and host carbonate; (2) metamorphic origin (Chen, 2006; Chen et al., 2007; Goldfarb et al., 2005; Zhong et al., 2013); and (3) magmatic origin in the porphyry-epithermal mineralization systems formed in intra-continental tectonic settings (Hedenquist and Henley, 1985; Chen and Fu, 1992; Chen and Li, 2009; Chen and Wang, 2011; Li et al., 2012a, 2012b; Yang et al., 2013; Wang et al., 2014; Chen et al., 2016). The carbonate sequences are absent in the Zijinshan orefield, which rules out the possibility of the first explanation. The Zijinshan Cu-Au deposit is a high-sulfidation epithermal deposit as indicated by the geological characteristics, which are believed to be genetically associated with the coeval magmatic-hydrothermal fluids, rather than the metamorphic solutions (Hedenquist and Lowenstern, 1994; Simmons et al., 2005; Sillitoe, 2010; Chen et al., 2007; Chen and Li, 2009). The magmatic origin of the ore-forming fluids in Zijinshan is further supported by the D-O stable isotopic compositions (Zhang et al., 1992; Hua et al., 1998; Zhou et al., 1998). In fact, the magmatic origin of ore-forming fluids in other HS epithermal systems is also confirmed, including the Rodalquilar, Spain (Arribas et al., 1995) and Lepanto, Philippine (Hedenquist et al., 1998). Heinrich (2005), Williams-Jones and Heinrich (2005) and Sillitoe (2010) proposed that the advanced argillic alteration (represented by the occurrence of alunite) is formed

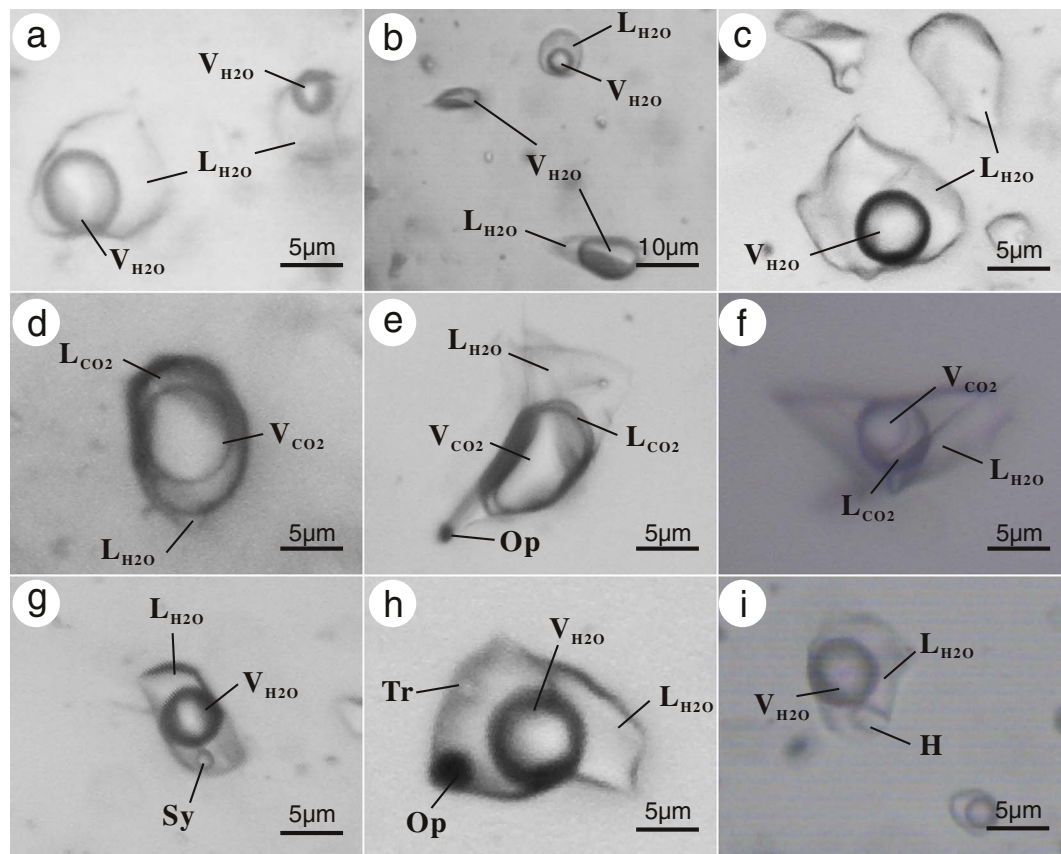


Fig. 7. Photomicrographs showing fluid inclusions in the Zijinshan deposit.

(a) Liquid-rich aqueous (WL-subtype) inclusions. (b) Coexistence of the liquid-rich (WL-subtype), vapor-rich (WV-subtype) and pure vapor aqueous inclusions with similar total homogenization temperatures (Th), implying fluid boiling process. (c) Liquid-rich (WL-subtype) and pure liquid aqueous inclusions developing in the healed intergranular microfractures in quartz grains from the Cu ore samples with alunite-dominated alteration, which are interpreted to be trapped from the ore-forming fluids of the Cu-Au mineralization stage. (d) Typical CO<sub>2</sub>-rich (C-type) inclusion in quartz of the alunite-dominated samples, with vapor phase accounting for > 90% in volume. (e) Solid bearing (SC-type) inclusion with vapor CO<sub>2</sub> (CO<sub>2</sub> phase is nearly 60% in volume) and an identified opaque daughter mineral. (f) Rare C-type inclusion with the CO<sub>2</sub> phase < 40%, of which the carbonic phase homogenized into liquid CO<sub>2</sub> upon heating. (g) SM-subtype inclusion with a sylvite daughter mineral in the alunite-dominated samples. (h) SM-subtype inclusion with both opaque and transparent daughter minerals. (i) Halite-bearing inclusions (SH-subtype).

Abbreviation: L<sub>H2O</sub>, H<sub>2</sub>O liquid; V<sub>H2O</sub>, H<sub>2</sub>O vapor; V<sub>CO2</sub>, CO<sub>2</sub> vapor; L<sub>CO2</sub>, CO<sub>2</sub> liquid; H, halite; Op, opaque mineral; Sy, sylvite; Tr, transparent daughter mineral.

synchronously to the underlying potassium alteration, which are resulted from the separated vapor phase and saline phase by fluid immiscibility from a single-phase, low- to moderate-salinity liquid of magmatic origin at depth.

The large amounts of the carbonic inclusions (C-type and SC-subtype) in the magmatic-hydrothermal fluids at the Zijinshan HS Cu-Au deposit are uncommon in most other epithermal mineralization systems worldwide, such as the Lepanto Cu-Au deposit in Philippine (Mancano and Campbell, 1995; Hedenquist et al., 1998), the Chinkuashih Au-Cu deposit in Taiwan, China (Wang et al., 1999; Wang, 2010), the Jinxi-Yelmand Au deposit and other high sulfidation systems in northern Xinjiang, China (Xiao et al., 2005; Chen et al., 2012), etc. Chen and Li (2009) indicated that the CO<sub>2</sub>-rich FIs in ore-forming fluids are diagnostic for those intrusion-related hypothermal deposits in intracrustal tectonic settings (e.g., Chen and Wang, 2011; Yang et al., 2012, 2013; Li et al., 2012b; Wang et al., 2014), and are resulted from the magmatic source of continental crust or lithospheric mantle with high CO<sub>2</sub>/H<sub>2</sub>O, K/Na, and F/Cl ratios. However, very few CO<sub>2</sub>-rich inclusions in the nearby Luoboling porphyry Cu-Mo deposit were identified (Zhong et al., 2011, 2014, 2017c), indicating that besides the magmatic origin in intracrustal setting, more parameters should be taken into consideration to decipher the CO<sub>2</sub> origin in the Zijinshan deposit.

Lowenstern (2000, 2001) suggested that the solubility of the CO<sub>2</sub> in granitic magma decreased at decreasing pressures and elevated

temperatures. Fogel and Rutherford (1990) and Blank et al. (1993) also demonstrated that CO<sub>2</sub> would be exsolved before H<sub>2</sub>O, Cl at higher pressures. Giggenschbach (1997) indicated that the effervescence in the granitic magma with 0.1 wt% CO<sub>2</sub> would occur at ~2 kbar, but the pressures would rise to > 20 kbar if the CO<sub>2</sub> content increased to 1 wt %. Therefore, the CO<sub>2</sub> contents in exsolved ore-forming fluids in the magmatic-hydrothermal mineralization systems seem to be largely affected by the emplacement depth of the causative magma; the deeper the causative magma intruded, the more CO<sub>2</sub> components could be exsolved. The nearby Luoboling Cu-Mo deposit is a shallow-seated porphyry mineralization system and the emplacement depth of the causative granodiorite porphyry is estimated to be ~4.1 km by aluminum-in-hornblende geobarometry (Zhong et al., 2014; D.P. Li et al., 2013). The mineralization depth of the Zijinshan Cu-Au deposit has already exceeded 1.5 km so far, yet the concealed porphyry is still unrevealed and a greater depth is suggested, which might be an important reason for the occurrence of CO<sub>2</sub> vapor-rich inclusions.

In addition, both the bulk (Zhang et al., 1992) and single fluid inclusion composition analyses (this study) indicated that the ore-forming fluids in the alunite alteration samples are rich in CO<sub>3</sub><sup>2-</sup> and HCO<sub>3</sub><sup>-</sup>. The ore-forming fluids are also suggested to be highly acid due to the disproportionation reaction of SO<sub>2</sub> (4SO<sub>2</sub> + 4H<sub>2</sub>O = 3H<sub>2</sub>SO<sub>4</sub> + H<sub>2</sub>S; Stoffregen, 1987; Williams-Jones and Heinrich, 2005). The CO<sub>2</sub> contents would largely increase due to the reaction between H<sup>+</sup> and CO<sub>3</sub><sup>2-</sup>, HCO<sub>3</sub><sup>-</sup> (2H<sup>+</sup> + CO<sub>3</sub><sup>2-</sup> = H<sub>2</sub>O + CO<sub>2</sub>; H<sup>+</sup> + HCO<sub>3</sub><sup>-</sup> = H<sub>2</sub>O

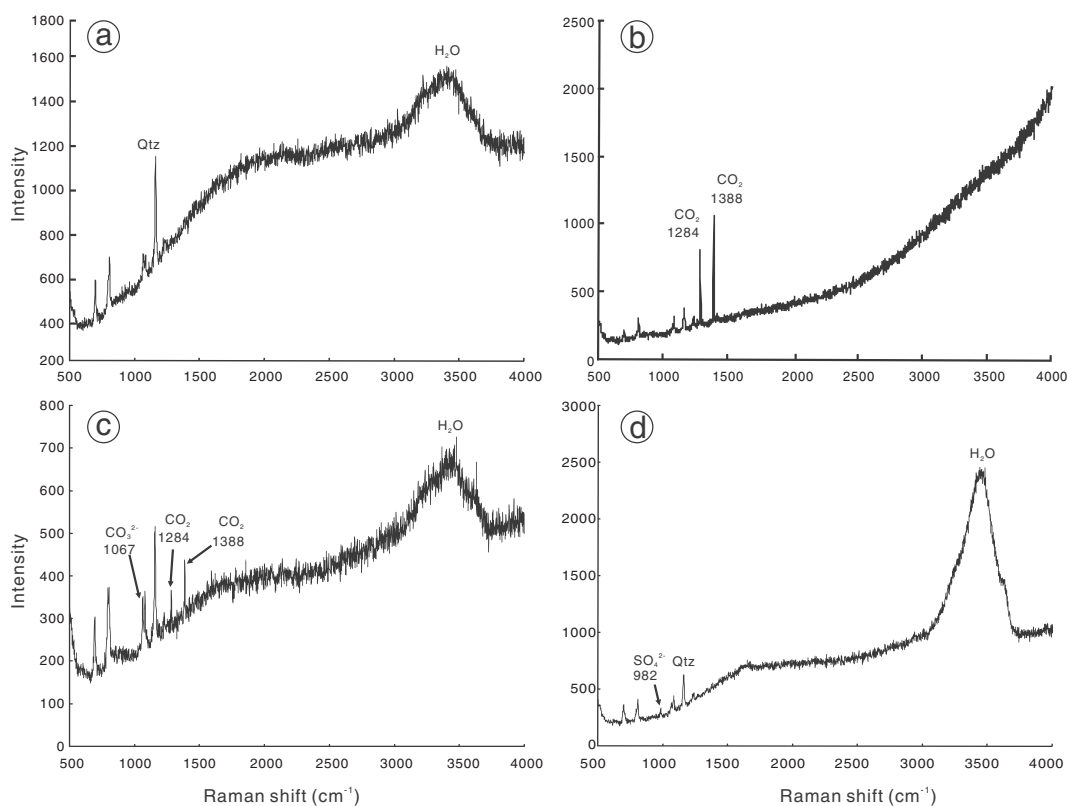


Fig. 8. Laser Raman spectra of fluid inclusions in Zijinshan.

(a) H<sub>2</sub>O-spectrum of the WL-subtype inclusion. (b) CO<sub>2</sub>-spectrum of the CO<sub>2</sub>-rich inclusions; (c) CO<sub>2</sub>-spectrum of the vapor and H<sub>2</sub>O-spectrum of the liquid of the C-type or SC-subtype inclusions, where a CO<sub>3</sub><sup>2-</sup> spectrum is also detected; (d) H<sub>2</sub>O, SO<sub>4</sub><sup>2-</sup>-spectra of the liquid from W-type inclusions from the alunite-dominated samples.

+ CO<sub>2</sub>) in the ore-forming fluids.

### 7.2. Origin and evolution process of the ore-forming fluids

The occurrences of the S- and C-type inclusions with total homogenization temperatures higher than 300 °C indicated that the ore-forming fluids related to the sericite (or porphyry mineralization) and alunite alteration are mainly magmatic fluids in origin. The FIs in the dickite (high-sulfidation Cu mineralization-related) and the silicic (Au mineralization-related, Zhang et al., 1992) alteration zones, however, are dominated by the liquid-rich aqueous inclusions with total homogenization temperatures below 300 °C, implying a meteoric-dominated origin. This is consistent with the stable isotopic compositions obtained

by Zhang et al., 1992, Hua et al., 1998 and Zhou et al., 1998 (Table 4; Fig. 12). The D-O systematic also indicated that the ore-forming fluids of the Cu-Au mineralization stage are meteoric water in origin.

Hedenquist and Henley (1985), Wilkinson (2001) and Canet et al. (2011) summarized the variation trend between the salinity and total homogenization temperature data for FIs underwent fluid dilution, boiling and cooling from high and low gas epithermal systems as shown in Fig. 10d. Trend 1 is the hypothetical result of the boiling of a gas-poor fluid, with continued boiling and steam loss resulting in a slight enrichment of the dissolved salts with cooling (a maximum of about 30% enrichment from adiabatic boiling and steam loss of a 300 °C fluid to 200 °C, Hedenquist and Henley, 1985). Trend 2 displays the simple cooling or pressurization trend, with no salinity change. Trend 3 shows

Table 3  
Microthermometric data of FIs in quartz from the Zijinshan Cu-Au deposit.

Dominated alteration	Type	N.	T <sub>m, CO2</sub> (°C)	T <sub>m, Cla</sub> (°C)	T <sub>m, ice</sub> (°C)	T <sub>m, NaCl</sub> (°C)	Th (°C)	Salinity (wt% NaCl)	Density (g/cm <sup>3</sup> )
Sericite	WL	226			-13.9 to -0.2		158–446	0.4–12.4	0.51–0.92
	WV	17			-2.5 to -0.2		212–458	0.7–9.9	0.47–0.85
	C	5	-56.8 to -56.6	5.7–8.8			262–421	2.4–8.0	0.39–0.52
	SH	6				213–393	213–393	32.5–46.7	1.07–1.13
	SC	6	-56.8 to -56.6	5.7–8.1			366–388	3.8–8.0	0.40–0.44
	SM	20			-8.2 to -0.1		170–389	0.2–11.9	0.64–0.90
Alunite	WL	225			-0.1 to -10.0		169–442	0.2–13.9	0.52–0.94
	WV	6					280–382		
	C	92	-57.7 to -56.6	1.1–9.6			210–424	0.2–15.3	0.29–1.01
	SC	5	-56.8 to -56.6	4.2–8.6			294–359	2.8–10.3	0.54–0.86
	SM	29			-0.8 to -9.8		169–383	1.4–13.7	0.61–0.95
Dickite	WL	56			-0.5 to -5.1		158–391	0.9–8.0	0.58–0.93
	WV	1			-0.8		350	1.4	0.59
	C	5	-56.8 to -56.6	1.5–9.9			238–334	2.6–6.6	0.85–0.91

Notations: N-number of FIs analyzed; T<sub>m, CO2</sub>, melting temperature of solid CO<sub>2</sub>; T<sub>m, Cla</sub>, melting temperature of clathrate; T<sub>m, ice</sub>, last ice-melting temperature; T<sub>m, NaCl</sub>, melting temperature of solid halite; Th, total homogenization temperature of all the phases in FIs.

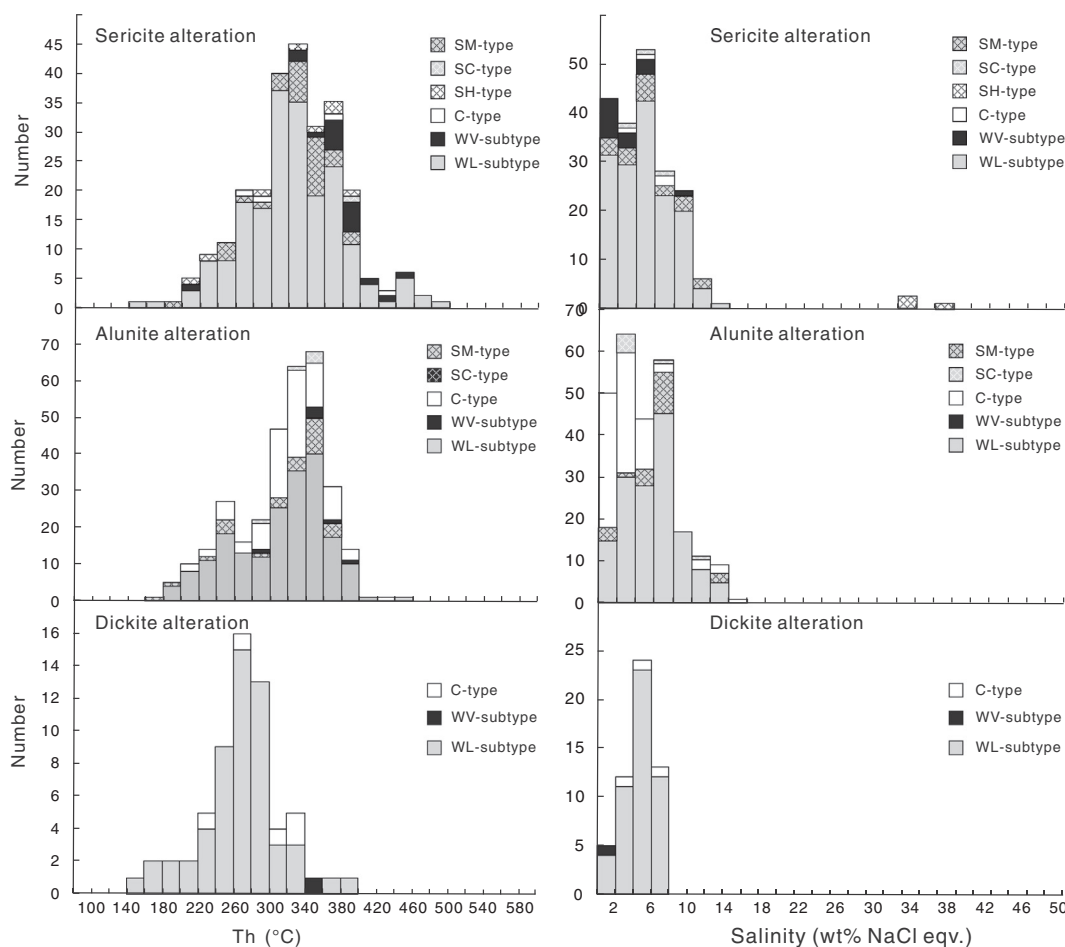


Fig. 9. Histograms of homogenization temperatures and salinities of FIs in different alteration zones from the Zijinshan Cu-Au deposit.

the dilution trend of a high temperature, high salinity end-member by cold groundwater, while trend 4 is explained by the result of boiling with effervescence in a volatile-rich system (e.g., CO<sub>2</sub>-bearing), where the salinities of inclusions are largely controlled by the CO<sub>2</sub> contents. The Th-salinity bivariate plot is used to decipher the mineralization mechanism and ore-forming processes for the ore-forming fluids in this study.

The earliest sericite alteration related to the porphyry Cu-Mo mineralization in the Zijinshan deposit is characterized by the typical fluid boiling assemblage, i.e., the high-salinity SH-subtype, relatively low-salinity vapor-rich WV-subtype, SC-subtype, C-type and liquid-rich WL-subtype inclusions with similar Th but contrasting salinities in a single quartz grain (Fig. 10a). The vapor-rich WV-, SC-subtype and C-type inclusions display a near-vertical salinity decrease trend with Th decrease, whereas the salinities of the liquid-rich WL-, SM-subtype inclusions are plotted into a broad range in the Th-salinity diagram (Fig. 10b), both showing the boiling or effervescence trend. The magmatic ore-forming fluids related to the sericite alteration are further diluted by the low-temperature, low-salinity meteoric water, as supported by the Th-salinity trend for the inclusions with Th below 300 °C and H-O isotopic compositions (Zhang et al., 1992; Hua et al., 1998; Zhou et al., 1998). Pervasive fluid boiling lead to the temperature decrease of the ore-forming system and vapor CO<sub>2</sub>, H<sub>2</sub>O escape, which are both favorable mechanisms for metal precipitation (Chen et al., 2007; Fan et al., 2011; Drummond and Ohmoto, 1985) and might trigger the formation of the chalcopyrite-bornite-molybdenite-pyrite veins or stockworks, although the mineralization scale might be limited.

Alunite alteration following the sericite alteration is also resulted from fluid boiling by magmatic-dominated fluids as shown by the

similar Th-salinity trend of the C-type, W-type and S-type inclusions with the sericite alteration (Fig. 10c), while the meteoric water-dominated dickite alteration might also be resulted from fluid boiling as indicated by the relatively broad salinity range with similar Th (Fig. 10d). Fluid boiling in the alunite alteration is further supported by the occurrence of the ore-hosting cryptoexplosive breccias (Fig. 3e, h), which are commonly related to the escape of vapor CO<sub>2</sub> (Chen et al., 2009; Fan et al., 2011; Li et al., 2012a). The formation of alunite is essentially resulted from the SO<sub>2</sub> disproportionation reaction (4SO<sub>2</sub> + 4H<sub>2</sub>O = 3H<sub>2</sub>SO<sub>4</sub> + H<sub>2</sub>S), producing isotopically light sulfide (commonly pyrite) and heavy sulfate (alunite) (Stoffregen, 1987). The alunite grains can be also formed from the transformation of sericite (e.g., Fig. 4e) by the reaction:



during which the hydrogen ions are largely consumed, resulting in the hydrolyzation of H<sub>2</sub>S and increase of the HS<sup>-</sup> contents in the residual ore-forming fluids. This would further lead to increase of the solubility of the Cu-Au complex and is not conducive for Cu-Au mineral precipitation. Although large-scale mineralization in the sulfate alteration (alunite alteration) stage is absent, the micro-fractures, fissures resulted from fluid boiling are favorable locations for later Cu-Au minerals.

Direct fluid inclusion analyses for the high sulfidation Cu-Au mineralization veins are absent in the Zijinshan deposit due to the lack of suitable minerals for microthermometric studies. However, a group of secondary inclusions intergrown with small enargite grains are recognized (Fig. 13) in the ore-hosting alunite alteration samples and present a normal distribution in the total homogenization histogram, with temperatures below 300 °C and peaking at 260–280 °C (Fig. 9).

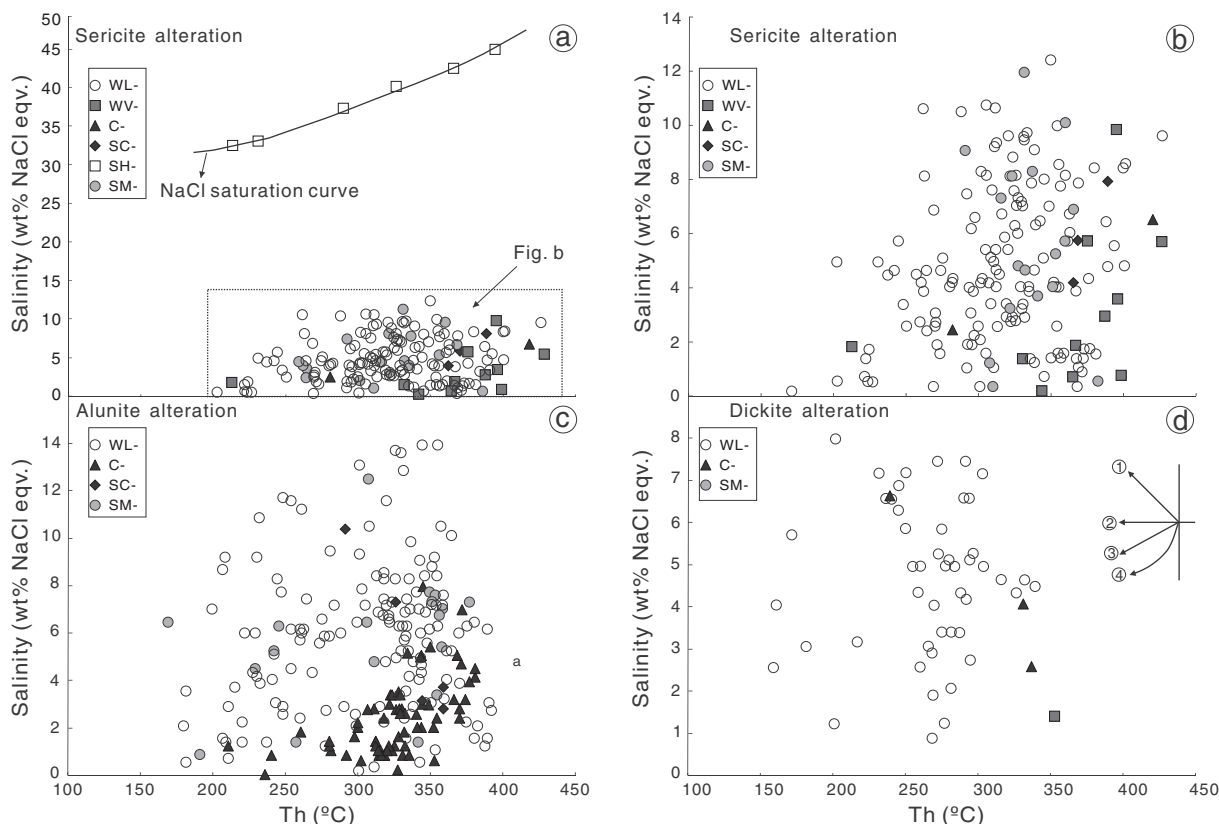


Fig. 10. Homogenization temperatures vs. salinities of fluid inclusions in different mineralization stage of the Zijinshan Cu-Au deposit.

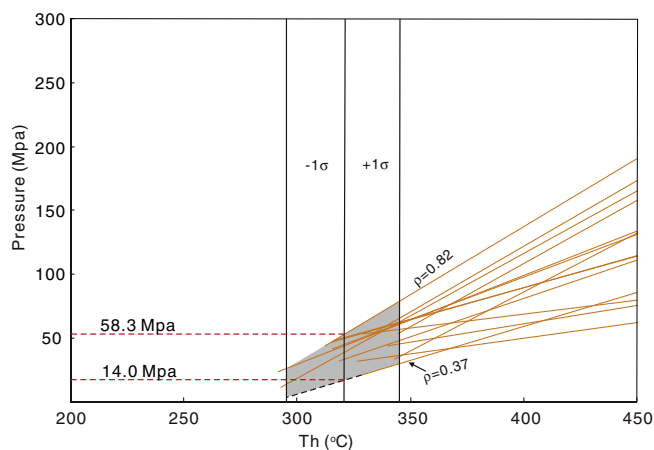


Fig. 11. The trapping pressure estimation diagram for Zijinshan deposit. The isochors of the C-type inclusions in the alunite-dominated samples are calculated using the Flincor program (Brown, 1989) and the formula of Bowers and Helgeson (1983). The average total homogenization used here is 325 °C.

The secondary FIs are therefore considered to be trapped from the ore-forming fluids in the Cu mineralization stage. The temperature of the FIs during the Cu mineralization stage below 300 °C is consistent to the thermal stability of the major gangue mineral dickite (Hedenquist et al., 2000) in the Cu sulfide-bearing veins or stockworks (Fig. 5e, f, i) and the homogenization temperatures of the samples from dickite alteration zone. The temperature range is also nearly identical to a few reported microthermometric results of the inclusions in enargite, including those in the Lepanto Cu-Au deposit, Philippine (166–285 °C, Mancano and Campbell, 1995) and Julcani deposit, Peru (201–320 °C, Deen et al., 1994). The major Cu-Au mineral precipitation is also attributed to fluid boiling as suggested by the temperature-salinity trend. The formation of major gangue mineral dickite would

increase the H<sup>+</sup> concentrations, probably by the reaction:  $2KAl_3(SO_4)_2(OH)_6 + 6SiO_2 + 3H_2O = 3Al_2Si_2O_5(OH)_4 + 2K^+ + 6H^+ + 4SO_4^{2-}$ , which would cause the formation of H<sub>2</sub>S by the association between H<sup>+</sup> and HS<sup>-</sup>, and further lead to the instability of bisulfide or sulfur complex of Cu-Au and the precipitation of Cu-Au minerals.

### 7.3. Possible location of the concealed porphyry mineralization

The advanced argillic alteration (characterized by the occurrence of alunite) is believed to be co-genetically and synchronously formed together with a concealed high-temperature potassium alteration and porphyry mineralization (Williams-Jones and Heinrich, 2005; Heinrich, 2005; Sillitoe, 2010), exemplified by the Lepanto-Far Southeast porphyry-epithermal mineralization system (Hedenquist et al., 1998). Therefore, it is commonly advocated that a porphyry mineralization system might be concealed at depth of the Zijinshan deposit (Zhang et al., 1992; Qiu et al., 2010; Liu et al., 2016), yet the exact location still remains ambiguous.

In this manuscript, the average total homogenization temperatures (Th) of each sample from drill core Nos. DZK702, DZK801 and DZK1202 are plotted on a cross section profile and the isotherms are constructed by Kriging interpolation method (Fig. 14). It is shown that the average Th decreases downward in all the three boreholes in vertical section, as well as from the southeastern volcanic edifice to the northwestern parts in plane section. The downward decreasing trend of Th is consistent with the thermal stability of dominant gangue minerals from alunite to dickite (c.f., Hedenquist et al., 2000). Wang and Jue (2013) systematically analyzed the alunite compositions in the Zijinshan deposit and it turns out that the Na contents decreases from the southeastern volcanic edifice northwestward. Stoffregen and Cygan (1990) suggested that the Na content in alunite is in positive correlation with its formation temperature, indicating a temperature decrease trend from southeast to northwest in Zijinshan. Moreover, Dai (2011)

**Table 4**  
The  $\delta D$  and  $\delta^{18}O$  ratios (‰) for the Zijinshan Cu–Au deposit.

Sample no.	Major mineralization or alteration	Mineral	$\delta^{18}O_Q$ (‰)	$\delta^{18}O_{H_2O}$ (‰)	$\delta D$ (‰)	Th (°C)	Data source
D2-2	Au ore	Qtz	13.99	0.89	−60.9	190	Zhang et al., 1992
D2-3	Silicified granite	Qtz	13.02	−5.17	−60	140	Zhang et al., 1992
Z-218	Silicified Au–Cu ore	Qtz	13.94	−4.25	−62.1	140	Zhang et al., 1992
Zj62	Silicified host rock	Qtz	14.7	−4.49	140	140	Zhang et al., 1992
Zj67	Dickite vein	Di	8.4	2.26	180	180	Zhang et al., 1992
Zj145	Silicified host rock	Qtz	14.2	−3.99	140	140	Zhang et al., 1992
Zj385	Host rocks with phyllic alteration	Qtz	10.8	1.16	250	250	Zhang et al., 1992
Z11	?	Qtz	12.85	6.9	−50.2	350	Hua et al., 1998
Z19	?	Qtz	10.16	5.95	−51.2	378	Hua et al., 1998
Z34	?	Qtz	9.69	−1.63	−48.9	218	Hua et al., 1998
Z36	?	Qtz	10.93	2.2	270	270	Hua et al., 1998
1	Host rocks with phyllic alteration	Qtz	10.8	0.4	−64	250	Zhou et al., 1998
2	Host rocks with alunite alteration	Qtz	13.99	2.5	−55	230	Zhou et al., 1998
3	Au–Cu ore	Qtz	13.94	4.5	−62.1	250	Zhou et al., 1998
4	Au ore	Qtz	13.99	2.5	−60.9	230	Zhou et al., 1998
5	Host rocks with dickite alteration	Qtz	8.4	−5.2	−108	250	Zhou et al., 1998
6	Host rocks with silicic alteration	Qtz	14.68	−5.6	−62.8	140	Zhou et al., 1998
7	Host rocks with silicic alteration	Qtz	14.35	−5.9	−60	140	Zhou et al., 1998

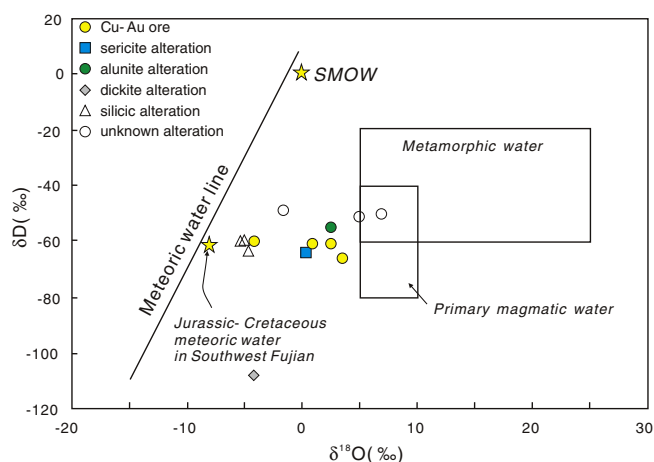


**Fig. 12.** The summarized  $\delta D$  –  $\delta^{18}O$  systematics for the Zijinshan Cu–Au deposit (after Taylor, 1974). The data are cited from Zhang et al. (1992), Hua et al. (1998) and Zhou et al. (1998).

and Liu et al. (2014) suggested that the element primary halos evolved from the high-temperature W–Cu element assemblage in the southeastern deep part to low-temperature Au–Ag–Hg–Bi element assemblage in the northwestern shallow region of the Zijinshan deposit, which is also in agreement with our microthermometric results.

Given the isotherms in this study, and considering that the ore-forming fluids are transported along the NW-trending faults or fractures, the major conducting structures should be the NW-trending faults or fractures above +520 m asl, while the possible heat source and the porphyry mineralization coeval to the high-sulfidation Cu–Au mineralization might be located either in the southeast of the Zijinshan deposit or in the north between the Zijinshan and Wuziqilong deposits at depth (Figs. 2a, 15), rather than in the southwestern Zijinshan at depth as illustrated by Zhang (2013). Recently, Duan et al. (2017) reported newly discovered porphyry Cu–Mo mineralization in the southeastern part of the Zijinshan deposit. This is very inspiring and more drilling work are encouraged to be carried out herein, and also the northern part between the Zijinshan and Wuziqilong deposits.

Since the major conduit faults or fractures is located above +520 m asl, the digenite- and covellite-dominated orebodies at depth of nearly −400 m asl are actually distal mineralization to the heat and mineralization center, which is in agreement with the pinching trend of the high-sulfidation Cu orebodies at depth of the drill cores (e.g., Fig. 2b). It is also believed that the variation from alunite to dickite

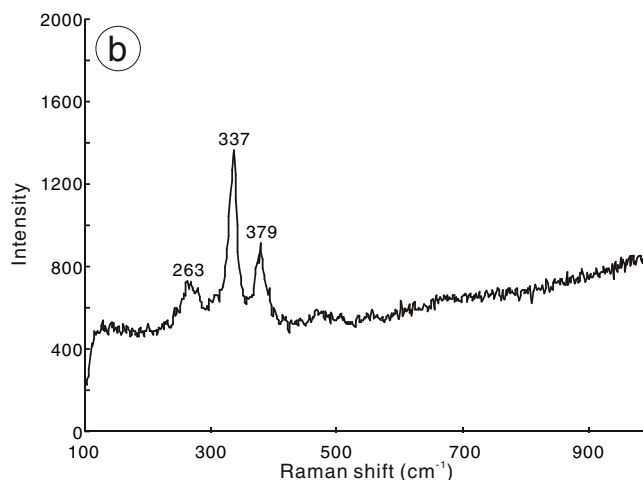
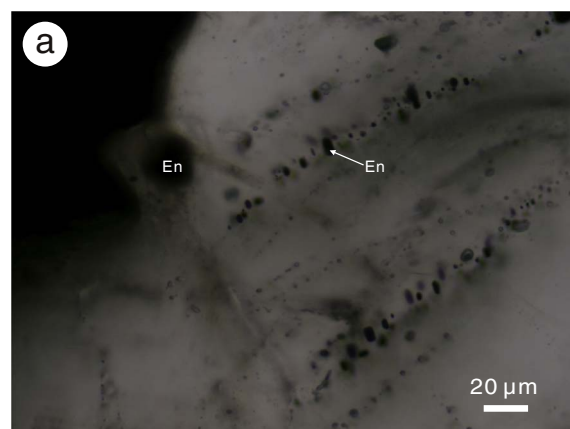


**Fig. 13.** (a) Photomicrograph showing enargite grains intergrown with secondary fluid inclusions in quartz grains in the alunite-dominated samples, indicating a common origin between the secondary inclusions and the Cu-sulfides. (b) Laser Raman spectrum of the largest enargite grain in a.

from center to distal region is largely controlled by the heat recession and acid component decrease outward. Hence, the vertical extend of the orebodies > 1.5 km does not represent the actual mineralization depth. However, as discussed in Section 6.4, the mineralization depth of the Zijinshan deposit ranges from 1.4 to 2.1 km, which is still beyond the maximum depth for other epithermal mineralization systems worldwide (Simmons et al., 2005; Hedenquist et al., 2000). We suggest

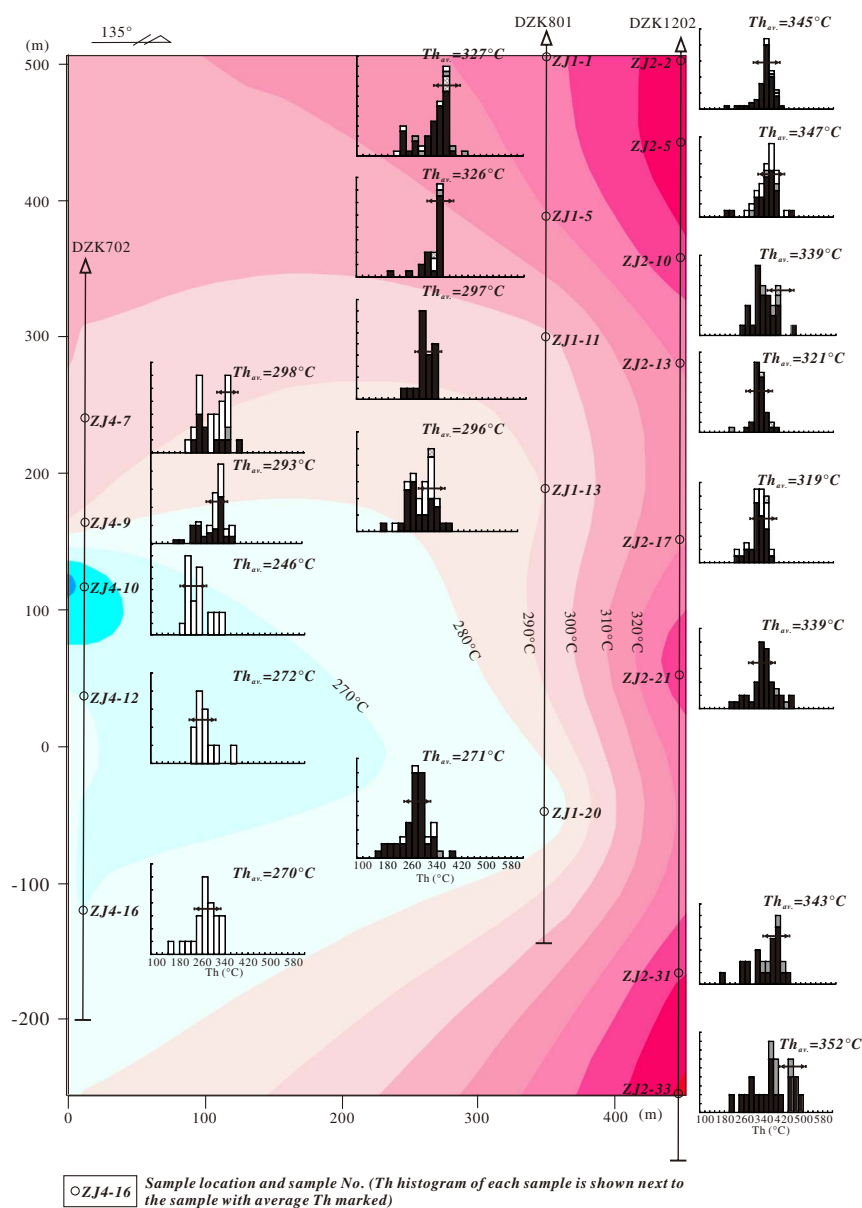


**Fig. 14.** Isotherms determined by the interpolation of microthermometric data of FIs from drill core Nos. DZK702, DZK801 and DZK1202. Average homogenization temperature of each sample is used and the effect of the post-mineralization movement of the NE-trending faults is not evaluated herein.

that the great mineralization depths at Zijinshan are resulted from the superposition of the high-sulfidation mineralization onto an early porphyry mineralization (see detail in Section 5).

**8. Conclusion**

1. Four mineralization stages are recognized in the Zijinshan Cu-Au deposit: porphyry Cu (chalcopyrite + bornite, related to sericite or phyllic alteration), the sulfate alteration, the high-sulfidation Cu-Au mineralization (associated with dickite alteration), and the later supergene leaching stages.
2. D-O isotope signatures, microthermometric results and LRS analyses of the fluid inclusions show that the ore-forming fluid system evolved from a high-temperature, high-salinity, CO<sub>2</sub>-rich magmatic in both the sericite (related to porphyry Cu mineralization) and alunite alteration zone to low-temperature, low-salinity, CO<sub>2</sub>-poor meteoric-dominated in the dickite alteration and Cu-Au mineralization stages. Intensive fluid boiling and possibly the replacement of the early-stage porphyry type Cu minerals resulted in the formation of giant high-sulfidation Cu (covellite-, digenite-dominated) orebodies in the deposit.

3. The mineralization depth of the Zijinshan Cu-Au deposit range from 1.4 to 2.1 km, exceeding the maximum depth of the epithermal mineralization system (1.5 km), which indicated that the Zijinshan deposit is a deep-seated epithermal deposit.
4. The isotherms constructed by the microthermometric data of FIs in cross section profile suggested that the heat source of the Zijinshan deposit might be located at the southeastern Zijinshan deposit or the northern area between the Zijinshan and Wuziqilong deposits, where concealed porphyry mineralization could be expected.

**Acknowledgements**

This study was financially supported by the National Science Foundation of China (No. 41502083) and Ministry of Science and Technology of the People's Republic of China (No. 2009BAB43B04). The field work is strongly supported by the Zijin Mining Co. Ltd. Drs. Richen Zhong and Yongfei Yang are thanked for their instructive discussion and suggestion. We are also grateful to Drs. Hongrui Fan, Xiaochun Li, Yachun Cai for their generous help in fluid inclusion analyses. Constructive suggestions and comments from two anonymous reviewers greatly improved the quality of the paper.

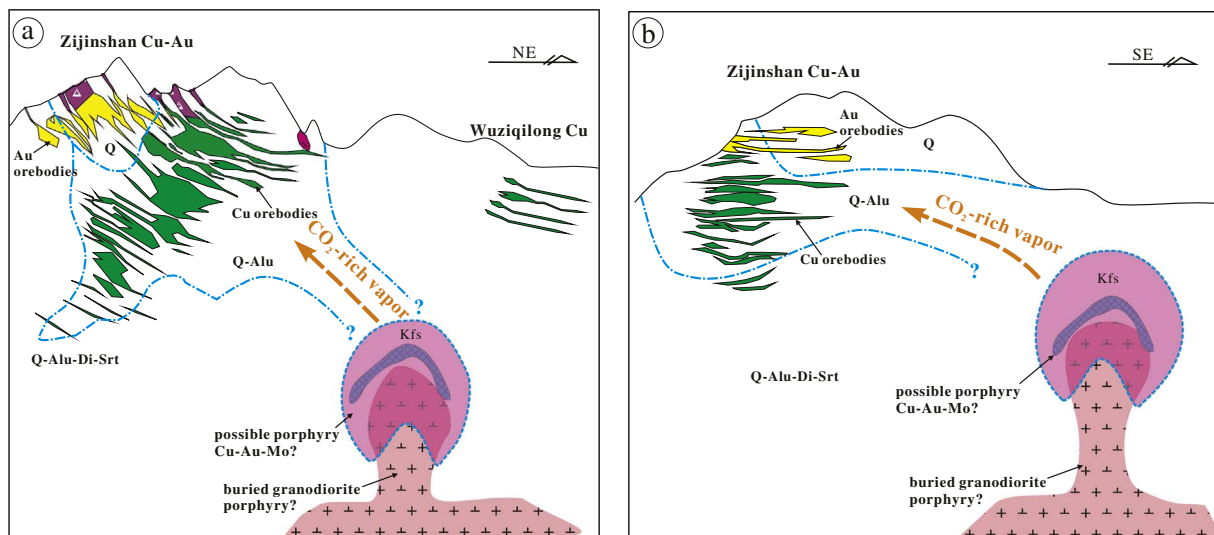


Fig. 15. The possible location of the concealed porphyry type mineralization and alteration at depth in the northern parts between the Zijinshan and Wuziqilong deposits (a) or at the southeastern Zijinshan deposit (b) (not to scale).

Abbreviations for alteration zones: Q, silicic alteration; Q-Alu, alunite alteration (or advanced argillic alteration); Q-Alu-Di-Srt, quartz-alunite alteration overprinting the sericite alteration.

## References

- Arribas Jr., A., Cunningham, C.G., Rytuba, J.J., Rye, R.O., Kelly, W.C., Podwysocski, M.H., Mckee, E.H., Tosdal, R.M., 1995. Geology, geochronology, fluid inclusions, and isotope geochemistry of the Rodalquilar gold alunite deposit, Spain. *Econ. Geol.* 90, 795–822.
- Blank, J.G., Stolper, E.M., Carroll, M.R., 1993. Solubilities of carbon dioxide and water in rhyolitic melt at 850 °C and 750 bar. *Earth Planet. Sci. Lett.* 119, 27–36.
- Bodnar, R.J., 1993. Revised equation and table for determining the freezing-point depression of H<sub>2</sub>O-NaCl solutions. *Geochim. Cosmochim. Acta* 57, 683–684.
- Bowers, T.S., Helgeson, H.C., 1983. Calculation of the thermodynamic and geochemical consequences of nonideal mixing in the system H<sub>2</sub>O-CO<sub>2</sub>-NaCl on phase relations in geologic systems: equation of state for H<sub>2</sub>O-CO<sub>2</sub>-NaCl at high pressures and temperatures. *Geochim. Cosmochim. Acta* 47, 1247–1275.
- Brown, P.E., 1989. Fliacor—a microcomputer program for the reduction and investigation of fluid-inclusion data. *Am. Mineral.* 74, 1390–1393.
- Canet, C., Franco, S.I., Prol-Ledesma, R.M., González-Partida, E., Villanueva-Estrada, R.E., 2011. A model of boiling for fluid inclusion studies: application to the Bolanos Ag-Au-Pb-Zn epithermal deposit, Western Mexico. *J. Geochem. Explor.* 110, 118–125.
- Chen, H.S., 1996. The research on the mineralization chronology and isotopic exploration assessment for Zijinshan copper-gold deposit. *Geotecton. Metallog.* 20, 348–360 (in Chinese with English abstract).
- Chen, J.H., 1999. The metallogenic model of Zijinshan copper-gold deposit. *Gold* 20, 6–11 (in Chinese with English abstract).
- Chen, Y.J., 2006. Orogenic-type deposits and their metallogenetic model and exploration potential. *Geol. China* 33, 1181–1196 (in Chinese with English abstract).
- Chen, J., 2013. Geological Features, Ore-forming Process of Epithermal Fluid Reformed Copper Deposit Systems in the Zijinshan Orefield, Fujian, China. Peking University, Beijing, pp. 1–75 (Master dissertation, in Chinese with English abstract).
- Chen, Y.J., Fu, S.G., 1992. Gold Mineralization in West Henan, China. China Seismological Press, Beijing, pp. 234 (in Chinese with English abstract).
- Chen, Y.J., Li, N., 2009. Nature of ore-fluids of intracontinental intrusion-related hypothermal deposits and its difference from those in island arcs. *Acta Petrol. Sin.* 25, 2477–2508 (in Chinese with English abstract).
- Chen, Y.J., Wang, Y., 2011. Fluid inclusion study of the Tangjiaping Mo deposit in Dabie Shan, Henan Province: implications for the nature of porphyry systems of postcollisional tectonic settings. *Int. Geol. Rev.* 53, 635–655.
- Chen, Y.J., Ni, P., Fan, H.R., Pirajno, F., Lai, Y., Su, W.C., Zhang, H., 2007. Diagnostic fluid inclusions of different types hydrothermal gold deposits. *Acta Petrol. Sin.* 23, 2085–2108 (in Chinese with English abstract).
- Chen, Y.J., Pirajno, F., Guo, D.S., Lai, Y., 2009. Isotope systematics and fluid inclusion studies of the Qiyugou breccia pipe-hosted gold deposit, Qinling Orogen, Henan Province, China: implication for ore genesis. *Ore Geol. Rev.* 35, 245–261.
- Chen, J., Chen, Y.J., Zhong, J., Sun, Y., Li, J., Qi, J.P., 2011. Fluid inclusion study of the Wuziqilong Cu deposit in the Zijinshan ore field, Fujian Province. *Acta Petrol. Sin.* 27, 1425–1438 (in Chinese with English abstract).
- Chen, Y.J., Pirajno, F., Wu, G., Qi, J.P., Xiong, X.L., 2012. Epithermal deposits in North Xinjiang, NW China. *Int. J. Earth Sci.* 101, 889–917.
- Chen, J., Chen, Y.J., Zhong, J., Sun, Y., Qi, J.P., Li, J., 2015. Geological and ore-fluid characteristics of Longjiangting Cu deposit in Zijinshan orefield, Fujian Province, and their genetic implications. *Mineral Deposits* 34, 98–118 (in Chinese with English abstract).
- Chen, Y.J., Wang, P., Li, N., Yang, Y.F., Pirajno, F., 2016. The collision-type porphyry Mo deposits in Dabie Shan, China. *Ore Geol. Rev.* <http://dx.doi.org/10.1016/j.oregeorev.2016.03.025>.
- Collins, P.L.F., 1979. Gas hydrates in CO<sub>2</sub>-bearing fluid inclusions and the use of freezing data for estimation of salinity. *Econ. Geol.* 74, 1435–1444.
- Dai, M.C., 2011. The Structural Characteristics of Primary Haloes in Boreholes and Prospecting Perspective in Depth of Zijinshan Copper-Gold Deposit, Fujian Province. China University of Geosciences (Wuhan), Wuhan, pp. 1–76 (Master dissertation, in Chinese with English abstract).
- Deen, J.A., Rye, R.O., Munoz, J.L., Drexler, J.W., 1994. The magmatic hydrothermal system at Julcani, Peru: evidence from fluid inclusions and hydrogen and oxygen isotopes. *Econ. Geol.* 89, 1925–1938.
- Diamond, L.W., 2001. Review of the systematics of CO<sub>2</sub>-H<sub>2</sub>O fluid inclusions. *Lithos* 55, 69–99.
- Drummond, S.E., Ohmoto, H., 1985. Chemical evolution and mineral deposition in boiling hydrothermal systems. *Econ. Geol.* 80, 126–147.
- Duan, G., Chen, H.Y., Hollings, P., Qi, J.P., Xu, C., Zhang, S., Xiao, B., Liu, G.Y., Liu, J.M., 2017. The Mesozoic magmatic sources and tectonic setting of the Zijinshan mineral field, South China: constraints from geochronology and geochemistry of igneous rocks in the Southeastern Ore Segment. *Ore Geol. Rev.* 80, 800–827.
- Fan, H.R., Hu, F.F., Wilde, S.A., Yang, K.F., Jin, C.W., 2011. The Qiyugou gold-bearing breccia pipes, Xiong'er shan region, central China: fluid inclusion and stable-isotope evidence for an origin from magmatic fluids. *Int. Geol. Rev.* 53, 25–45.
- Fogel, R.A., Rutherford, M.J., 1990. The solubility of carbon dioxide in rhyolitic melts: a quantitative FTIR study. *Am. Mineral.* 75, 1311–1326.
- Fournier, R.O., 1999. Hydrothermal processes related to movement of fluid in plastic into brittle rock in the magmatic-epithermal environment. *Econ. Geol.* 94, 1193–1211.
- Giggenbach, W.F., 1997. The origin and evolution of fluids in magmatic-hydrothermal systems. In: Barnes, H.L. (Ed.), *Geochemistry of Hydrothermal Ore Deposits*. John Wiley & Sons, Inc., New York, pp. 737–789.
- Goldfarb, R.J., Baker, T., Dube, B., Groves, D.I., Hart, C.J.R., Gosselin, P., 2005. Distribution, character, and genesis of gold deposits in metamorphic terranes. *Econ. Geol.* 407–450 (100th Anniversary Volume).
- Heald, P., Hayba, D.O., Foley, N.K., 1987. Comparative anatomy of volcanic-hosted epithermal deposits: acid-sulfate and adularia-sericite types. *Econ. Geol.* 82, 1–26.
- Hedenquist, J.W., 1987. Mineralization associated with volcanic-related hydrothermal systems in the Circum-Pacific basin. In: *Transactions of the Fourth Circum Pacific Conference on Energy and Mineral Resources*, Singapore. American Association of Petroleum Geologists, pp. 513–524.
- Hedenquist, J.W., Henley, R.W., 1985. The importance of CO<sub>2</sub> on freezing-point measurements of fluid inclusions—evidence from active geothermal systems and implications for epithermal ore deposition. *Econ. Geol.* 80, 1379–1406.
- Hedenquist, J.W., Lowenstern, J.B., 1994. The role of magmas in the formation of hydrothermal ore deposits. *Nature* 370, 519–527.
- Hedenquist, J.W., Arribas, A., Reynolds, T.J., 1998. Evolution of an intrusion-centered hydrothermal system: far Southeast-Lepanto porphyry and epithermal Cu-Au deposits, Philippines. *Econ. Geol.* 93, 373–404.
- Hedenquist, J.W., Arribas, A.R., Gonzalez-Urien, E., 2000. Chapter 7 exploration for epithermal gold deposit. *SEG Rev.* 13, 245–277.
- Heinrich, C.A., 2005. The physical and chemical evolution of low-salinity magmatic fluids at the porphyry to epithermal transition: a thermodynamic study. *Mineral. Deposita* 39, 864–889.
- Hu, C.J., Huang, W.T., Bao, Z.W., Liang, H.Y., Wang, C.L., 2012. LA-ICP-MS zircon U-Pb dating of the dacite porphyry from Zijinshan Cu-Au deposit and its metallogenetic implications. *Geotecton. Metallog.* 36 (2), 284–292 (in Chinese with English abstract).

- abstract).
- Hua, R.M., Hu, J.H., Huang, Y.S., Li, Z.M., 1998. Fluid migration-reaction model of Zijinshan deposit as traced by variation of oxygen isotope compositions. *Geochimica* 27, 187–195 (in Chinese with English abstract).
- Jiang, S.H., Liang, Q.L., Bagas, L., Wang, S.H., Nie, F.J., Liu, Y.F., 2013. Geodynamic setting of the Zijinshan porphyry-epithermal Cu–Au–Mo–Ag ore system, SW Fujian Province, China: constraints from the geochronology and geochemistry of the igneous rocks. *Ore Geol. Rev.* 53, 287–305.
- Jiang, S.H., Bagas, L., Liang, Q.L., 2017. Pyrite Re–Os isotope systematics at the Zijinshan deposit of SW Fujian, China: constraints on the timing and source of Cu–Au mineralization. *Ore Geol. Rev.* 80, 612–622.
- Li, B., Jiang, S.Y., 2015. A subduction-related metasomatically enriched mantle origin for the Luoboling and Zhongliao Cretaceous granitoids from South China: implications for magma evolution and Cu–Mo mineralization. *Int. Geol. Rev.* 57, 1239–1266.
- Li, N., Carranza, E.J.M., Ni, Z.Y., Guo, D.S., 2012a. The CO<sub>2</sub>-rich magmatic fluid of the Qiyugou breccia pipe, Henan Province, China: implication for breccia genesis and gold mineralization. *Geochem. Explor. Environ. Anal.* 12, 147–160.
- Li, N., Ulrich, T., Chen, Y.J., Thomsen, T.B., Pease, V., Pirajno, F., 2012b. Fluid evolution of the Yuchiling porphyry Mo deposit, East Qinling, China. *Ore Geol. Rev.* 48, 442–459.
- Li, B., Zhao, K.D., Yang, S.Y., Dai, B.Z., 2013a. Petrogenesis of the porphyritic dacite from Ermaogou Cu–Au deposit in Zijinshan orefield and its metallogenic implications. *Acta Petrol. Sin.* 29, 4167–4185 (in Chinese with English abstract).
- Li, D.P., Qiu, X.P., Zhang, W.H., Liu, W.Y., 2013b. The SHRIMP U–Pb ages and mineralization depth of the volcanic rocks and porphyries in the Zijinshan Orefield, Fujian Province, China. *Acta Mineral. Sin.* 592–593 (suppl., in Chinese).
- Li, B., Zhao, K.D., Xu, Y.M., Zhu, Z.Y., 2015. Petrogenesis and geochemical characteristics of the Zijinshan granitic complex from Fujian Province, South China. *Acta Petrol. Sin.* 31 (3), 811–828 (in Chinese with English abstract).
- Liu, Y., Liu, W.Y., Wang, S.H., 2011. Preliminary compositional investigation of binary Cu sulfides from Zijinshan Cu–Au deposit. *Mineral Deposits* 30, 735–741 (in Chinese with English abstract).
- Liu, G.Y., Dai, M.C., Qi, J.P., Zhang, J.Z., 2014. Geochemical characteristics of primary halos and ore-search prospecting in the depth of the Zijinshan copper-gold deposit, Fujian Province. *Geophys. Geochem. Explor.* 38, 434–440 (in Chinese with English abstract).
- Liu, W.Y., Cook, N.J., Ciobanu, C.L., Liu, Y., Qiu, X.P., Chen, Y.C., 2016. Mineralogy of tin-sulfides in the Zijinshan porphyry-epithermal system, Fujian Province, China. *Ore Geol. Rev.* 72, 682–698.
- Lowenstern, J.B., 2000. A review of the contrasting behavior of two magmatic volatiles: chlorine and carbon dioxide. *J. Geochem. Explor.* 69–70, 287–290.
- Lowenstern, J.B., 2001. Carbon dioxide in magmas, implications for hydrothermal systems. *Mineral. Deposita* 36, 490–502.
- Lu, H.Z., Fan, H.R., Ni, P., Ou, G.X., Shen, K., Zhang, W.H., 2004. Fluid Inclusion. Science Press, Beijing (in Chinese).
- Mancano, D.P., Campbell, A.R., 1995. Microthermometry of enargite-hosted fluid inclusions from the Lepanto, Philippines, high-sulfidation Cu–Au deposit. *Geochim. Cosmochim. Acta* 59, 3909–3916.
- Mao, J.R., Tao, K.Y., Li, J.Y., Xie, F.G., Xu, N.Z., 2002. Geochronology and geochemical characteristics in late Mesozoic Sifang pluton, southwestern Fujian, and their significance. *Acta Petrol. Sin.* 18, 449–458 (in Chinese with English abstract).
- Pirajno, F., 2009. *Hydrothermal Processes and Mineral System*. Springer, Berlin, pp. 1250.
- Qiu, X.P., Lan, Y.Z., Liu, Y., 2010. The key to the study of deep mineralization and the evaluation of ore-prospecting potential in the Zijinshan gold and copper deposit. *Acta Geosci. Sin.* 31, 209–215 (in Chinese with English abstract).
- Sillitoe, R.H., 2010. Porphyry copper systems. *Econ. Geol.* 105, 3–41.
- Simmons, S.F., White, N.C., John, D.A., 2005. Geological characteristics of epithermal precious and base metal deposits. *Econ. Geol.* 485–522 (100th Anniversary Volume).
- So, C.S., Zhang, D.Q., Yun, S.T., Li, D.X., 1998. Alteration-mineralization zoning and fluid inclusions of the high sulfidation epithermal Cu–Au mineralization at Zijinshan, Fujian Province, China. *Econ. Geol.* 93, 961–980.
- Stoffregen, R., 1987. Genesis of acid-sulfate alteration and Au–Cu–Ag mineralization at Summitville, Colorado. *Econ. Geol.* 82, 1575–1591.
- Stoffregen, R.E., Cygan, G.L., 1990. An experimental study of Na–K exchange between alunite and aqueous sulfate solutions. *Am. Mineral.* 75, 209–220.
- Taylor, H.P., 1974. The application of oxygen and hydrogen isotope studies to problems of hydrothermal alteration and ore deposition. *Econ. Geol.* 69, 843–883.
- Wang, Y.S., 2010. Physical and chemical characteristics of the host rocks in controlling the mineralization of the Chinkuashih high-sulfidation gold-copper deposits, north-eastern Taiwan. *J. Geochem. Explor.* 104, 61–68.
- Wang, C.Z., Jue, H.H., 2013. Mineralogical characteristics of alunite from Zijinshan gold-copper deposit. *Acta Mineral. Sin.* 33, 329–336 (in Chinese with English abstract).
- Wang, Y.S., Sasaki, M., Sasada, M., Chen, C.H., 1999. Fluid inclusion studies of the Chinkuashih high-sulfidation gold-copper deposits in Taiwan. *Chem. Geol.* 154, 155–167.
- Wang, P., Chen, Y.J., Fu, B., Yang, Y.F., Mi, M., Li, Z.L., 2014. Fluid inclusion and H–O–C isotope geochemistry of the Yaochong porphyry Mo deposit in Dabie Shan, China: a case study of porphyry systems in continental collision orogens. *Int. J. Earth Sci.* 103, 777–797.
- Wilkinson, J.J., 2001. Fluid inclusions in hydrothermal ore deposits. *Lithos* 55, 229–272.
- Williams-Jones, A.E., Heinrich, C.A., 2005. Vapor transport of metals and the formation of magmatic-hydrothermal ore deposits. *Econ. Geol.* 1287–1312 (100th Anniversary Volume).
- Wu, L.Y., Hu, R.Z., Qi, Y.Q., Zhu, J.J., 2013. Zircon LA-ICP-MS U–Pb ages and geochemical characteristics of quartz syenite porphyry from Jintonghu deposit in Zijinshan orefield, Fujian Province, South China. *Acta Petrol. Sin.* 29, 4151–4166 (in Chinese with English abstract).
- Xiao, L., Hayward, N., Begg, G., Fu, M.L., Wang, F.Z., Pirajno, F., 2005. The Jinxi-Yelmand high-sulfidation epithermal gold deposit, western Tianshan, Xinjiang Province, P.R. China. *Ore Geol. Rev.* 26, 17–37.
- Yang, Y.F., Li, N., Chen, Y.J., 2012. Fluid inclusion study of the Nannihu giant porphyry Mo–W deposit, Henan Province, China: implications for the nature of porphyry ore-field systems formed in a continental collision setting. *Ore Geol. Rev.* 46, 83–94.
- Yang, Y.F., Chen, Y.J., Li, N., Mi, M., Xu, Y.L., Li, F.L., Wan, S.Q., 2013. Fluid inclusion and isotope geochemistry of the Qian'echong giant porphyry Mo deposit, Dabie Shan, China: a case of NaCl-poor, CO<sub>2</sub>-rich fluid systems. *J. Geochem. Explor.* 124, 1–13.
- Zhang, J.Z., 2013. Geology, exploration model and practice of Zijinshan ore concentrated area. *Mineral Deposits* 32, 757–766 (in Chinese with English abstract).
- Zhang, D.Q., Li, D.X., Zhao, Y.M., Chen, J.H., Li, Z.L., Zhang, K.Y., 1992. Alteration and Mineralization Zoning of the Zijinshan Copper-Gold Deposit. Geological Publishing House, Beijing (77 pp, in Chinese).
- Zhang, D.Q., She, H.Q., Yan, S.H., Xu, W.Y., 2001. Geochemistry of Mesozoic magmatites in the Zijinshan region and implication on regional tectonic inversion. *Geol. Rev.* 47, 608–616 (in Chinese with English abstract).
- Zhang, D.Q., Fen, C.Y., Li, D.X., She, H.Q., Dong, Y.J., 2003a. <sup>40</sup>Ar–<sup>39</sup>Ar dating of adularia from Bitian sericite-adularia type epithermal Ag–Au deposit in Fujian Province and its geological significance. *Mineral Deposits* 22, 360–364 (in Chinese with English abstract).
- Zhang, D.Q., She, H.Q., Li, D.X., Feng, C.Y., 2003b. The porphyry-epithermal metallogenic system in the Zijinshan. *Acta Geol. Sin.* 77, 253–261 (in Chinese with English abstract).
- Zhao, X.L., 2007. The Geochronology, Petrography and Geochemical Characteristics of Mesozoic Granitoids From Shanghang Area in SW Fujian and Their Implications. Chinese Academy of Geological Sciences, Beijing, pp. 1–57 (Master dissertation, in Chinese with English abstract).
- Zhao, X.L., Mao, J.R., Chen, R., Xu, N.Z., 2008. SHRIMP zircon dating of the Zijinshan pluton in southwestern Fujian and its implications. *Geol. China* 35, 590–597 (in Chinese with English abstract).
- Zhong, J., Chen, Y.J., Chen, J., Li, J., Qi, J.P., Dai, M.C., 2011. Fluid inclusion study of the Luoboling porphyry Cu–Mo deposit in the Zijinshan orefield, Fujian Province. *Acta Petrol. Sin.* 27, 1410–1424 (in Chinese with English abstract).
- Zhong, R.C., Li, W.B., Chen, Y.J., Yue, D.C., Yang, Y.F., 2013. P–T–X conditions, origin, and evolution of Cu-bearing fluids of the shear zone-hosted Huogeqi Cu–(Pb–Zn–Fe) deposit, northern China. *Ore Geol. Rev.* 50, 83–97.
- Zhong, J., Chen, Y.J., Pirajno, F., Chen, J., Li, J., Qi, J.P., Li, N., 2014. Geology, geochemistry, fluid inclusion and H–O isotope geochemistry of the Luoboling porphyry Cu–Mo deposit, Zijinshan orefield, Fujian Province, China. *Ore Geol. Rev.* 57, 61–77.
- Zhong, J., Pirajno, F., Chen, Y.J., 2017a. Epithermal deposits in South China: geology, geochemistry, geochronology and tectonic setting. *Gondwana Res.* 42, 193–219.
- Zhong, J., Chen, Y.J., Qi, J.P., Chen, J., Dai, M.C., Li, J., 2017b. Geology, fluid inclusion and stable isotope study of the Yueyang low-sulfidation Ag–Au–Cu deposit, Zijinshan orefield, Fujian Province, China. *Ore Geol. Rev.* 86, 254–270.
- Zhong, J., Chen, Y.J., Pirajno, F., 2017c. Geology, geochemistry and tectonic settings of the molybdenum deposits in South China: a review. *Ore Geol. Rev.* 81, 829–855.
- Zhou, S., Chen, H.S., 1996. Geochronology and geological significance of the Zijinshan copper-gold deposit. *Bull. Mineral. Petrol. Geochem.* 15 (04), 216–219 (in Chinese with English abstract).
- Zhou, S., Qiu, R.Z., Chen, H.S., 1998. Characteristics of hydrogen and oxygen isotopic composition of the Zijinshan copper-gold deposit and the relation to the ore-forming process. *Fujian* 2, 94–100 (in Chinese with English abstract).
- Zijin Mining Group Co., 2001. Exploration Report in the Northwestern Section of the Zijinshan Cu–Au Deposit. Fujian Province. Unpublished report, Shanghang County (in Chinese).